UNIVERSITY OF OKLAHOMA

GRADUATE COLLEGE

DEVELOPMENT AND CHARACTERIZATION OF DIW 3D PRINTED EPOXY SYNTACTIC FOAM FOR LIGHTWEIGHT STRUCTURAL APPLICATIONS

A THESIS

SUBMITTED TO THE GRADUATE FACULTY

in partial fulfillment of the requirements for the

Degree of

MASTER OF SCIENCE

By DAVIN KEON RHULE

Norman, Oklahoma

2025

DEVELOPMENT AND CHARACTERIZATION OF DIW 3D PRINTED EPOXY SYNTACTIC FOAM FOR LIGHTWEIGHT STRUCTURAL APPLICATIONS

A THESIS APPROVED FOR THE

SCHOOL OF AEROSPACE AND MECHANICAL ENGINEERING

BY THE COMMITTEE CONSISTING OF

Dr. Mrinal Saha, Chair

Dr. Yijie Jiang

Dr. Jingyao Dai

Acknowledgements

First, I would like to acknowledge Dr. Mrinal. C. Saha for providing an opportunity for me to work in his research group at the University of Oklahoma. His constant support through not only my academic journey but also my own personal well-being encouraged me every day that achieving this dream was possible. In many ways, my life kickstarted during my graduate studies and Dr. Saha stood by me in more ways than one that provided a platform for my success for which I will always be grateful. I would also like to thank Dr. Yijie Jiang and Dr. Dai for graciously serving on my committee. Their insights and encouragement gave me an extra push across the finish line when things got a little difficult. Additionally, this achievement would not be possible without my amazing lab partners. I would like to express my heartfelt thanks to Anirban Mondal, Dr. Mohammad Abshirini, Emmanuel Hakizimana, Omkar Gautam, and Dr. Kuntal Maity for their continuous support. I am also thankful to Dr. Preston Larson for his help with SEM related matters. To Billy Mays, Greg Williams and everyone at the AME machine shop, thank you for always finding solutions to every new idea or problem I presented. Lastly, I my heart goes out to my family – my mom, dad, and sisters for always uplifting me and reminding me that I am more than able to accomplish my goals.

Dedication

I would like to dedicate this thesis to my beautiful wife, Langelihle Dlamini. Without her, I'm not sure I would have enjoyed this chapter as much as I did. Proverbs 18:22 says, "He who finds a wife finds a good thing and obtains favor from the LORD." Every day that I wake up, I realize how true that is. My wife has been my rock, my comfort, and above all, my best friend through thick and thin. This master's degree is a culmination of the trust and belief that she placed in me and for that, I will forever be thankful and overjoyed I get to share this achievement with her for the rest of my life.

Lastly, I would like to dedicate the end of this journey to my Lord and savior Jesus Christ. Thank you, Lord, for being faithful even when I lacked faith. Help me to always remember:

Hebrews 11:1 - Now faith is the assurance of things hoped for, the conviction of things not seen.

Table of Contents

Table of Figures

Table of Tables

Abstract

The development of lightweight materials with high specific strength and energy absorption capability is critical for advancing structural applications in aerospace, automotive, and defense industries. Syntactic foams, composed of hollow glass microballoons (GMBs) embedded within a polymer matrix, have emerged as promising candidates for such applications due to their tunable mechanical properties and low density. However, conventional fabrication methods such as casting present significant challenges when processing highly viscous, particle-filled epoxy systems, often leading to defects, voids, and limited geometric control.

This research focuses on the development, processing, and mechanical characterization of 3D printable epoxy-based syntactic foam inks reinforced with hollow glass microballoons using Direct Ink Writing (DIW) technology. Three different types of GMBs from 3M: S60, iM16K, and iM30K, were incorporated into EPON 815C epoxy resin with Epikure 3230 curing agent. Rheological modifiers, including fumed silica and thixotropic additives, were used to tailor the ink's shear-thinning behavior and yield stress for printability. Rheological characterization using a Discovery HR-30 Rheometer confirmed that all inks exhibited desirable shear-thinning behavior, while yield stress values varied depending on microballoon type. The iM16K ink exhibited the highest yield stress due to its highest volume fraction of microballoons resulting from its lower density and smaller particle size.

Mechanical characterization was performed on both cast and 3D printed specimens. Tensile testing of 3D printed dogbone specimens in 0°, 45°, and 90° orientations revealed print orientation-dependent mechanical behavior, with the 0° orientation generally producing the highest tensile modulus, while strength varied depending on defect sensitivity and interlayer bonding. Compressive testing was conducted on cube specimens printed in both unidirectional

and bidirectional print patterns and tested in the X- and Y-directions to evaluate anisotropy. Printed samples exhibited more consistent mechanical performance compared to cast specimens, which suffered from voids and inconsistencies due to the challenges of casting highly viscous inks.

Ultimately, hybrid ink formulations were developed by combining iM16K and iM30K microballoons in different ratios (3:1, 2:2, and 1:3) to optimize specific strength and specific modulus. The iM30K_2 iM16K_2 hybrid ink emerged as the optimal formulation, exhibiting the highest balance of specific mechanical properties and superior crashworthiness parameters, including energy absorption (EA), specific energy absorption (SEA), mean crushing force (MCF), and peak crushing force (PCF).

Finally, the optimized hybrid ink was used to design, and 3D print hexagonal honeycomb core structures with 30% infill density. In-plane compression testing revealed direction-dependent behavior, with the Y-direction exhibiting higher peak compressive strength due to loading along inclined walls, while the X-direction showed slightly higher stiffness. These results validated the capability of DIW 3D printing to fabricate architected epoxy syntactic foam structures with tailored mechanical performance suitable for lightweight, energy-absorbing applications.

This research provides a comprehensive framework for the formulation, processing, and evaluation of DIW 3D printed syntactic foams, contributing to the advancement of lightweight structural materials for future engineering applications.

Chapter 1: Introduction

1.1 Background

Lightweight materials play a critical role in modern engineering applications, particularly in industries such as aerospace, automotive, marine, and energy, where reducing structural weight without sacrificing mechanical performance is essential for improving fuel efficiency, energy savings, and overall performance [1, 2]. Among various classes of lightweight materials, syntactic foams have emerged as a promising candidate due to their unique combination of low density and enhanced mechanical properties.

Syntactic foams are a class of composite materials consisting of hollow particles, often referred to as microballoons or microspheres, embedded within a polymer, metal, or ceramic matrix [3]. The inclusion of hollow particles significantly reduces the density of the material while providing tailored mechanical properties such as compressive strength, stiffness, and energy absorption capability. The properties of syntactic foams can be engineered by varying the type, size, volume fraction, and properties of the hollow particles, as well as by modifying the matrix material.

Epoxy-based syntactic foams have gained widespread attention due to their superior chemical resistance, low shrinkage, good mechanical properties, and compatibility with a wide range of fillers [4, 5]. The use of hollow glass microballoons (GMBs) within an epoxy matrix is one of the most common approaches for achieving lightweight foams with high specific strength and stiffness.

Traditionally, syntactic foams have been fabricated using casting or molding processes. However, these methods present several challenges when producing complex geometries or structures with controlled internal architectures. Casting high-viscosity, particle-filled materials often results in issues such as poor particle dispersion, void formation, and limited design flexibility.

Recent advancements in additive manufacturing (AM) technologies, particularly Direct Ink Writing (DIW), have enabled new possibilities for the fabrication of syntactic foams. DIW is an extrusion-based 3D printing technique capable of depositing highly viscous, particle-laden inks in a layer-by-layer manner, allowing for the creation of complex geometries, tailored architectures, and tunable mechanical properties [6, 7]. DIW also enables control over print paths and filament orientations, allowing researchers to study anisotropic behavior in printed structures.

Despite the growing interest in DIW of syntactic foams, there remain challenges in formulating printable inks that balance flowability during extrusion with structural stability after deposition. Rheological behavior, including viscosity, yield stress, and viscoelastic properties, plays a critical role in determining printability and final part quality. Moreover, the mechanical performance of printed syntactic foams depends on multiple factors, including microballoon type, volume fraction, print orientation, and processing conditions [8].

This research aims to contribute to the growing field of 3D printed syntactic foams by developing epoxy-based DIW inks reinforced with hollow glass microballoons. Through comprehensive rheological characterization, mechanical testing, and structural evaluation, this work seeks to explore the relationships between material formulation, processing, and mechanical behavior, with the ultimate goal of enabling lightweight, mechanically efficient structures for advanced engineering applications.

1.2 Research Gap & Motivation

Despite the growing interest in Direct Ink Writing (DIW) of syntactic foams, several critical research gaps remain unaddressed. Existing literature on printable epoxy-based syntactic foam inks is limited, particularly in the context of formulations designed for structural applications that demand both low density and high mechanical performance. Additionally, there is a lack of comprehensive studies examining the combined effects of microballoon type, particle size, and hybrid microballoon formulations on the rheological behavior and mechanical properties of DIW-printed syntactic foams. The influence of print orientation, filament alignment, and resulting anisotropic mechanical behavior — especially under tension- and compression-dominated loading conditions — also remains underexplored. Furthermore, there is a notable absence of systematic investigations that integrate rheological characterization, mechanical performance evaluation, and practical application of printed syntactic foams in architected structures such as honeycomb cores. Addressing these gaps is essential to advancing the use of DIW for the fabrication of lightweight, mechanically efficient syntactic foam structures suitable for engineering applications.

The motivation for this research is to address these knowledge gaps by developing a DIW 3D printable epoxy syntactic foam ink system reinforced with hollow glass microballoons, aimed at lightweight structural applications. This work seeks to provide a comprehensive study of:

- The influence of microballoon type and hybrid formulations on rheological behavior and printability.

- The mechanical performance of printed syntactic foam structures under tensile and compressive loading conditions, considering the effect of print orientation and architecture.
- The design and evaluation of 3D printed hexagonal honeycomb core structures using the optimized hybrid ink to validate its potential for lightweight energy-absorbing applications.

By addressing these objectives, this research aims to advance the understanding of DIW of thermoset-based syntactic foams and contribute to the development of novel lightweight materials suitable for aerospace, automotive, marine, and defense applications where weight savings and mechanical efficiency are critical.

1.3 Research Objectives

The primary objective of this research is to develop and characterize 3D printable epoxy syntactic foam inks reinforced with hollow glass microballoons (GMBs) using Direct Ink Writing (DIW) technology for lightweight structural applications. This study aims to explore the influence of material formulation, processing parameters, and print architecture on the mechanical performance of printed syntactic foam structures.

The first objective of this work is to formulate printable epoxy-based inks using EPON 815C resin and Epikure 3230 hardener, incorporating three different types of hollow glass microballoons (S60, iM16K, and iM30K) to study the effect of microballoon size, density, and crush strength on printability and mechanical behavior. To enable successful extrusion and shape retention during printing, rheological modifiers such as fumed silica and thixotropic additives were incorporated to tailor the ink's flow characteristics.

The second objective is to perform detailed rheological characterization of each ink formulation. This includes conducting steady-state flow tests to assess shear-thinning behavior and amplitude sweep tests to determine storage modulus, loss modulus, and yield stress, which are critical parameters governing DIW printability.

The third objective is to fabricate tensile and compression test specimens using DIW, and to evaluate the mechanical properties of printed syntactic foams. Tensile testing was performed on dogbone specimens printed in 0°, 45°, and 90° orientations, while compression testing was conducted on cube specimens printed in unidirectional and bidirectional patterns, tested in both the X- and Y-directions to evaluate anisotropic mechanical behavior.

The fourth objective is to develop hybrid ink formulations by combining iM16K and iM30K microballoons in varying ratios to optimize specific strength and specific modulus for lightweight structural applications. In addition to tensile and compressive property evaluation, crashworthiness parameters such as energy absorption (EA), specific energy absorption (SEA), mean crushing force (MCF), peak crushing force (PCF), and crush force efficiency (CFE) were calculated for hybrid ink compression specimens to assess their energy-absorbing capability.

Finally, the fifth objective is to apply the optimized hybrid ink formulation to design and 3D print hexagonal honeycomb core structures with a 30% infill density. In-plane compression testing was performed in both the X- and Y-directions to validate the performance of the developed material in architected lightweight structures suitable for energy-absorbing and load-bearing applications.

Chapter 2: DIW 3D Printable Ink Formulations and Printing Process

2.1 Introduction

The development of 3D printable inks suitable for Direct Ink Writing (DIW) of epoxy-based syntactic foams requires careful consideration of material formulation, processing methods, and printing parameters. The key objective of this chapter was to formulate and prepare epoxy syntactic foam inks that can be successfully extruded through a nozzle-based system while maintaining adequate structural integrity during and after printing.

In this study, epoxy syntactic foam inks were developed using EPON 815C epoxy resin and Epikure 3230 curing agent as the matrix material, combined with hollow glass microballoons (GMBs) to achieve lightweight properties. Three different types of GMBs were utilized: S60, iM16K, and iM30K, each with varying particle sizes, densities, and crush strengths to explore their influence on printability and mechanical performance. The selection of glass microballoons and their respective weight fractions were designed to balance density reduction with adequate strength and stiffness.

A critical challenge in the preparation of DIW inks for syntactic foams lies in achieving the desired rheological behavior — specifically, high viscosity at low shear rates to retain the printed shape (shape fidelity) and shear-thinning behavior to facilitate smooth extrusion through the nozzle [9, 10, 11]. The incorporation of GMBs into the epoxy resin significantly alters the flow behavior of the ink, necessitating rheological characterization to evaluate viscosity-shear rate relationships and yield stress behavior.

This chapter presents the procedures used for ink formulation, the materials utilized, and the characterization methods employed to assess the rheological properties of each ink. Additionally, the 3D printing process used for fabricating all specimens including the DIW printer setup, printing parameters, and print orientation strategies is outlined in this chapter. The outcomes of this chapter provided the necessary foundation for subsequent mechanical testing and evaluation of the developed syntactic foam materials discussed in later chapters.

2.2 Experimental

2.2.1 Materials

The epoxy syntactic foam inks developed in this study were prepared using a combination of commercially available materials selected to achieve suitable printability and mechanical performance for Direct Ink Writing (DIW) of lightweight structures.

The epoxy matrix consisted of EPON^{TM} 815C resin and Epikure^{TM} 3230 curing agent, both procured from Westlake Epoxy (formerly Hexion Inc.). This epoxy system was selected due to its low viscosity and favorable processing characteristics for particulate-filled composites.

Hollow glass microballoons (GMBs) were incorporated as the primary filler to reduce the density of the syntactic foam while maintaining structural integrity. Three different grades of glass microballoons, all procured from 3M™, were used in this study and their details listed in the table below:

Table 1: Microballoon Specifications

Microballoon Type	Average Diameter (μm)	True Density (g/cm^3)	Crush Strength (psi)	Wall Thickness (μm)
S60	30	0.60	10,000	1.49
iM16K	20	0.46	16,000	0.72
iM30K	15.3	0.60	28,000	0.70

To tailor the rheological behavior of the inks for DIW printability, fumed silica procured from Evonik Industries, was incorporated to promote shear-thinning behavior and enhance shape retention of the extruded filaments. Additionally, a thixotropic additive paste (TAP) was used to further control the viscoelastic response of the ink, improve structural stability after deposition, and prevent slumping or spreading of the printed features.

The combination of these materials including the epoxy resin, glass microballoons, fumed silica, and TAP, enabled the formulation of 3D printable inks with tunable rheological and mechanical properties suitable for fabricating lightweight, structurally efficient syntactic foam components using the DIW process.

2.2.2 Ink Formulation

The preparation of the 3D printable epoxy syntactic foam inks involved a multi-step mixing process designed to ensure uniform dispersion of all components while minimizing damage to the fragile glass microballoons. All materials were measured based on the desired weight fractions, and the ink formulation process was kept consistent across all base and hybrid inks developed in this study.

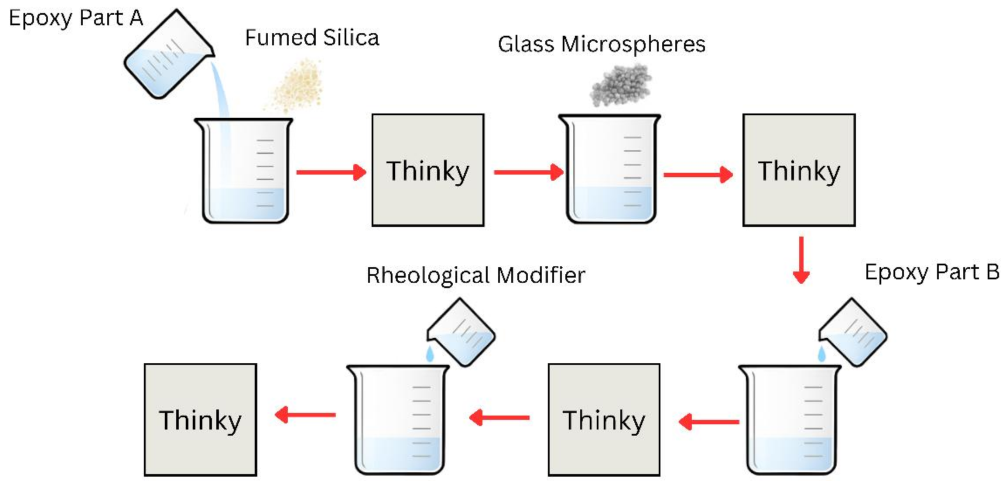

Figure 1: Ink Preparation Procedure

Figure 1 above shows the ink preparation procedure. First, the EPON™ 815C epoxy resin was measured into a mixing container according to the total required batch size. Fumed silica was then added at 1 wt% relative to the weight of the epoxy resin to act as a rheological modifier and enhance the shear-thinning behavior of the ink. The epoxy and fumed silica were initially hand-mixed using a spatula to achieve preliminary wetting and dispersion, followed by high-speed mixing using a Thinky AR-100 planetary mixer for 1 minute to ensure uniform distribution.

Following the dispersion of fumed silica, the appropriate type and amount of glass microballoons (S60, iM16K, iM30K, or hybrid combinations) were gradually introduced into the epoxy-fumed silica mixture for 40 wt% relative to the weight of epoxy. The glass microballoons were carefully added in small increments while gently hand-mixing to minimize breakage and ensure even distribution. This gradual addition process was repeated until the total desired weight of microballoons was incorporated.

Once the glass microballoons were fully integrated, the Epikure™ 3230 curing agent was added to the mixture at the manufacturer-recommended ratio of 3.13:1 (epoxy to hardener by weight).

The mixture was hand-mixed thoroughly to incorporate the curing agent and then mixed using the Thinky mixer for an additional 1 minute to achieve homogeneity.

Finally, a small amount of thixotropic additive paste (TAP) was added to further enhance the viscoelastic behavior of the ink, providing additional structural stability and preventing filament slumping after deposition. The TAP was first, hand-mixed into the ink, followed by a final 1-minute Thinky mixing cycle to ensure uniform dispersion.

The prepared ink was then transferred into a Nordson 10 mL syringe for degassing. The syringe containing the ink was degassed for 3 minutes to remove entrapped air bubbles introduced during the mixing process. After degassing, the ink was loaded into the DIW 3D printer and was ready for the printing process described in later sections. Once the specimens were printed, they were then cured in a programmable oven at 80 °C for 2 hours then 125 °C for 3 hours as per the manufacturer's instructions.

2.3 Rheological Characterization

2.3.1 Testing Procedure

Rheological characterization of the formulated epoxy syntactic foam inks was conducted to evaluate their flow behavior, printability, and viscoelastic properties, which are critical parameters for Direct Ink Writing (DIW) processes. All rheological tests were performed using a Discovery HR-30 Rheometer (TA Instruments).

The rheometer was equipped with a 40 mm parallel plate geometry at the top and a temperature-controlled Peltier stainless steel plate at the bottom to maintain a consistent testing environment throughout the experiments. A fixed gap of 1000 μm was carefully maintained between the upper and lower plates to securely hold the ink sample during testing and minimize the risk of slippage or edge effects.

Two primary tests were conducted on each ink formulation: steady-state flow tests and amplitude sweep tests. Steady-state flow tests were carried out to evaluate the viscosity and flow behavior of the inks over a shear rate range of 10^{-2} to 30 s^{-1}, which represents the expected shear rate conditions experienced during extrusion in the DIW process. The viscosity-shear rate data provided insight into the shear-thinning characteristics of each ink formulation, a desirable behavior for 3D printing applications. All flow tests were performed at a controlled temperature of 20°C to ensure consistent comparisons between inks.

Additionally, amplitude sweep tests were performed to assess the viscoelastic properties of the inks, particularly the storage modulus (G') and loss modulus (G") as a function of shear stress. These tests were used to determine the linear viscoelastic region (LVR) of each ink and to identify the yield stress, the critical shear stress at which the material transitions from an elastic solid-like behavior to a viscous flow behavior.

2.3.2 Rheology Results

The viscosity versus shear rate response for all three base ink formulations (S60, iM16K, and iM30K) is shown in Figure 2. All ink formulations exhibited pronounced shear-thinning behavior, a desirable characteristic for Direct Ink Writing (DIW) processes [12]. Shear-thinning materials display high viscosity at low shear rates, which helps maintain the shape fidelity of printed structures after deposition. At higher shear rates, the viscosity decreases significantly, facilitating smooth extrusion through the nozzle during printing.

As shown in the figure, the S60 ink consistently exhibited the lowest viscosity across the entire shear rate range tested. This result is attributed to the larger particle size of the S60 glass microballoons, which results in a lower total surface area available for particle-matrix interactions, thereby reducing the resistance to flow.

The iM16K ink demonstrated intermediate viscosity behavior, with values higher than the S60 ink but lower than the iM30K ink. This trend corresponds to the smaller particle size and higher surface area of the iM16K microballoons, leading to increased particle-matrix interaction and higher resistance to flow at lower shear rates.

The iM30K ink exhibited the highest viscosity among all the inks tested. This is primarily due to the smallest particle size of the iM30K glass microballoons (15.3 µm), which results in the highest particle surface area and therefore the strongest interaction with the epoxy matrix and thixotropic additives. Additionally, the higher crush strength of the iM30K microballoons may contribute to a more rigid particle network, further enhancing the material's resistance to flow.

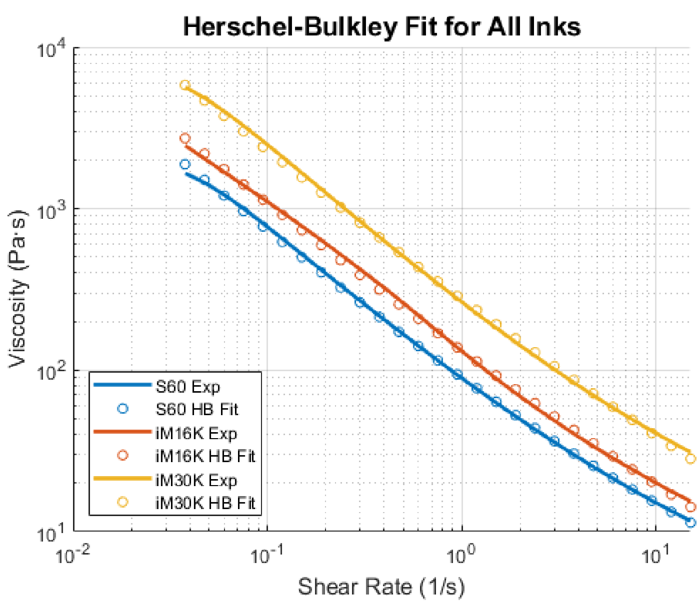

Figure 2: Viscosity vs Shear Rate for All Base Inks

Figure 2 also shows the corresponding Herschel-Bulkley (HB) model fits for the experimental data. The HB model is given by the equation:

$$\eta = \frac{\tau_0}{\dot{\gamma}} + K\dot{\gamma}^{(n-1)} \qquad \text{Eq. 1}$$

This equation was used to describe the non-Newtonian flow behavior of each ink. Here, τ_0 is the yield stress (Pa), K is the consistency index (Pa·s^n), and n is the flow behavior index. The fitted curves closely matched the experimental data across the tested shear rate range, confirming that the HB model effectively captures the shear-thinning behavior of the inks. In this context, a flow index $n = 1$ corresponds to Newtonian behavior, $n < 1$ indicates shear-thinning (pseudoplastic) behavior, and $n > 1$ represents shear-thickening behavior. All three inks exhibited shear-thinning characteristics consistent with $n < 1$, which is favorable for extrusion-based 3D printing applications such as direct ink writing (DIW). The results are shown in the table below.

Table 2: Rheological Parameters Summary

Inks	r (mm)	Shear Rate ($\dot{\gamma}$) (s^{-1})	K (Pa·s^n)	n	τ_0 Pa	τ Pa
S60	0.21	195.12	22.45	0.56	67.56	497.87
iM16K	0.21	195.12	38.73	0.42	93.32	448.11
iM30K	0.21	195.12	75.17	0.41	200.00	853.23

Table 2 presents a summary of the rheological parameters for the S60, iM16K, and iM30K inks. The wall shear rate ($\dot{\gamma}$) during printing was estimated using the relation:

$$\dot{\gamma} = \frac{4v}{r} \quad \text{Eq. 2}$$

where *v* is the print speed and *r* is the nozzle radius, taken as 0.21 mm for all inks. The Herschel-Bulkley model parameters *K* (consistency index), *n* (flow behavior index), and τ_0 (yield stress) were extracted from curve fits to experimental viscosity versus shear rate data using MATLAB. These parameters were then used to compute the wall shear stress (τ) during printing using the Herschel-Bulkley equation:

$$\tau = \tau_0 + K\dot{\gamma}^n \quad \text{Eq. 3}$$

Among the three inks, iM30K exhibited the highest yield stress (200.00 Pa) and wall shear stress (853.23 Pa), indicating greater resistance to flow compared to S60 and iM16K. While τ_0 captures the threshold stress required to initiate flow, the total wall shear stress τ includes the additional viscous contribution that dominates at high shear rates. Notably, although iM16K has a higher *K* than S60, its lower *n* value leads to a slightly lower τ highlighting the impact of flow behavior index on stress under printing conditions.

Furthermore, despite the differences in absolute viscosity values, all inks showed a consistent decrease in viscosity with an increasing shear rate, confirming their shear-thinning behavior. This rheological response is essential for DIW printing, as it ensures that the ink remains solid-like when stationary to maintain printed shape but flows readily under shear during extrusion.

The viscoelastic behavior of the inks, including storage modulus (G') and loss modulus (G"), as well as yield stress results from amplitude sweep tests can be seen in Figure 3 below.

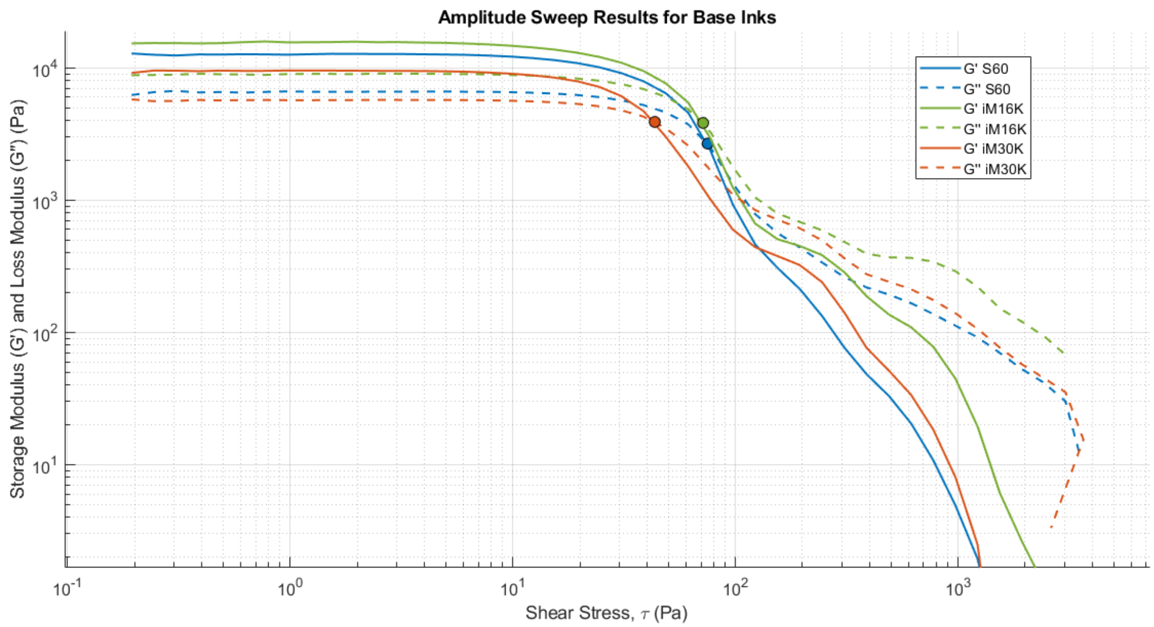

Figure 3: Amplitude Sweep showing Storage (G') and Loss (G'') Modulus vs Shear Stress (Pa) for all Base Inks

The amplitude sweep results for all three base ink formulations are shown in Figure 3, which presents the storage modulus (G') and loss modulus (G'') as a function of shear stress. These tests were conducted to evaluate the viscoelastic behavior of the inks and to determine their yield stress which is the critical shear stress at which the material transitions from a predominantly elastic (solid-like) response to a viscous (liquid-like) flow behavior [13, 14].

Across all inks, the storage modulus (G') remained relatively constant at low shear stresses, indicating a stable internal structure within the linear viscoelastic region (LVR). As the applied shear stress increased, a sharp decrease in G' was observed, signifying the breakdown of the internal structure and the onset of flow behavior. The yield stress for each ink was identified at the crossover point between G' and G'', indicating the stress required to initiate flow.

Among the three ink formulations, S60 exhibited the highest apparent yield stress of 75.016 Pa based on the amplitude sweep crossover point (where $G' = G''$). Interestingly, this contrasts with its fitted yield stress ($\tau_0 = 67.56\ Pa$) from the Herschel-Bulkley (HB) model, though the two values are reasonably close. The relatively high yield stress of S60 is notable given its larger microballoon size (30 μm) and lower volume fraction due to its higher density (0.60 g/cc), suggesting that strong surface interactions and packing efficiency may compensate for fewer particles. The iM16K ink showed a similar yield stress of 71.561 Pa from the amplitude sweep, with a slightly higher HB model yield stress of 93.32 Pa. The iM16K microballoons have a lower density (0.46 g/cc), which, given the fixed weight fraction, results in a higher number of particles per unit volume. This elevated volume fraction promotes more frequent particle-particle interactions, forming a more interconnected network that resists flow. The iM30K ink displayed the lowest dynamic yield stress of 43.420 Pa and the highest HB model yield stress of 200.00 Pa. This apparent discrepancy reflects the limitations of comparing dynamic (oscillatory) and steady shear yield behaviors. While iM30K has the highest crush strength and smallest particle size, its higher density reduces the volume fraction, limiting structural interaction and leading to earlier yielding under small-strain oscillations, despite requiring a high stress to sustain steady flow.

These results illustrate that amplitude sweep-derived yield stress and HB model yield stress (τ_0) represent different but complementary aspects of ink behavior: the former indicates the onset of nonlinearity or internal structure breakdown under small oscillatory strains, while the latter reflects the stress needed to initiate and sustain steady flow. Both metrics are important for DIW processing: the dynamic yield stress governs printability and shape fidelity, while the HB yield stress impacts extrusion performance and flow resistance. Together, the results highlight the significant roles of microballoon volume fraction, particle density, and matrix-filler interactions in tuning the rheological performance of syntactic foam inks.

2.4 3D Printing Process

2.4.1 Printer Specifications

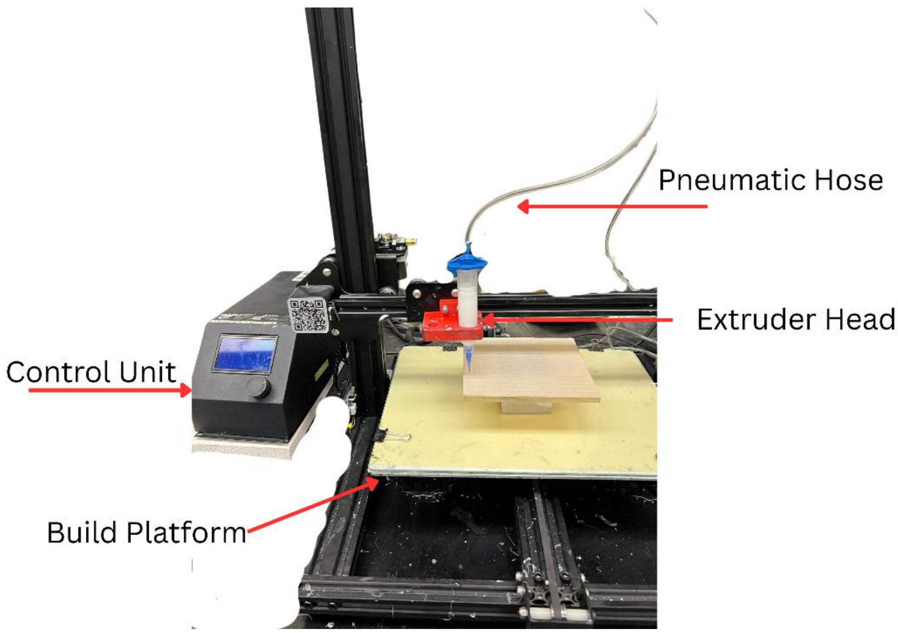

Figure 4: DIW 3D Printer Experimental Set-Up

A custom-built Direct Ink Writing (DIW) 3D printer was utilized for the fabrication of all epoxy syntactic foam specimens in this study. The DIW printer was modified from a commercially available Fused Deposition Modeling (FDM) 3D printer platform (Creality Ender 3), as shown in Figure 4.

The base FDM printer provided the necessary motion control system, including the control unit, build platform, and gantry system capable of precise three-axis movement. The original thermoplastic extrusion system was replaced with a pneumatic-driven material extrusion setup, suitable for printing high-viscosity epoxy-based inks.

Material extrusion was achieved using a pneumatic system connected via a flexible pneumatic hose to a custom-designed extruder head mounted on the printer carriage. The extruder head securely held a 10 mL Nordson syringe containing the formulated ink. Pneumatic pressure was supplied to the syringe to drive ink extrusion through a nozzle with a controlled inner diameter.

The build platform provided a flat surface for deposition and layer-by-layer fabrication of the printed structures. The printer was operated using G-code instructions generated from the part design, allowing precise control over print speed, layer height, nozzle path, and extrusion conditions.

This customized DIW setup enabled the extrusion of high-viscosity, particle-laden inks required for epoxy syntactic foams while leveraging the existing motion control capabilities of the original FDM printer framework. The ability to retrofit a standard FDM printer for DIW applications provided a cost-effective and flexible platform for research and development of printable composite materials.

2.4.2 Printing Parameters

All 3D printing of epoxy syntactic foam specimens in this study was conducted using the custom-built Direct Ink Writing (DIW) printer described in the previous section. To ensure consistency and repeatability across all printed specimens, a standardized set of printing parameters was maintained throughout the fabrication process.

A nozzle with an inner diameter of 410 μm was used for all prints. This nozzle size was selected to provide a balance between minimizing the risk of nozzle clogging, particularly for particle-filled inks, while maintaining sufficient print resolution and structural integrity of the deposited filaments.

The print speed was set at a constant rate of 10 mm/s for all specimens. This print speed was chosen to accommodate the shear-thinning behavior of the formulated inks and to ensure continuous, defect-free extrusion during printing.

Pneumatic pressure was applied to drive ink extrusion from the syringe reservoir, with the air pressure ranging from 3 to 13 psi depending on the specific ink formulation and print geometry. Inks with higher viscosity, such as those containing smaller microballoons (iM30K), required higher extrusion pressures within this range to overcome flow resistance and ensure stable material deposition.

All printing was conducted under ambient laboratory conditions at room temperature without the use of heated build platforms or controlled environmental chambers. This approach allowed for the evaluation of the intrinsic printability, flow behavior, and shape retention capability of the developed epoxy syntactic foam inks under standard atmospheric conditions.

The combination of optimized rheological properties, controlled air pressure, appropriate nozzle sizing, and slow print speeds enabled the reliable fabrication of tensile, compressive, and honeycomb structures suitable for subsequent mechanical characterization.

2.4.3 Print Orientations

Two primary print strategies were employed for the fabrication of compression specimens: uni-directional and bi-directional print patterns. These print patterns were designed to investigate the influence of filament orientation on the mechanical performance of 3D printed epoxy syntactic foam specimens.

Figure 5 illustrates the print paths used for unidirectional and bidirectional specimens. In the uni-directional print strategy (Figure 5 (a)), each layer consisted of continuous parallel lines deposited in a single direction, specifically along the Y-axis. All 13 layers of the unidirectional specimens were printed in the same orientation without rotation between layers.

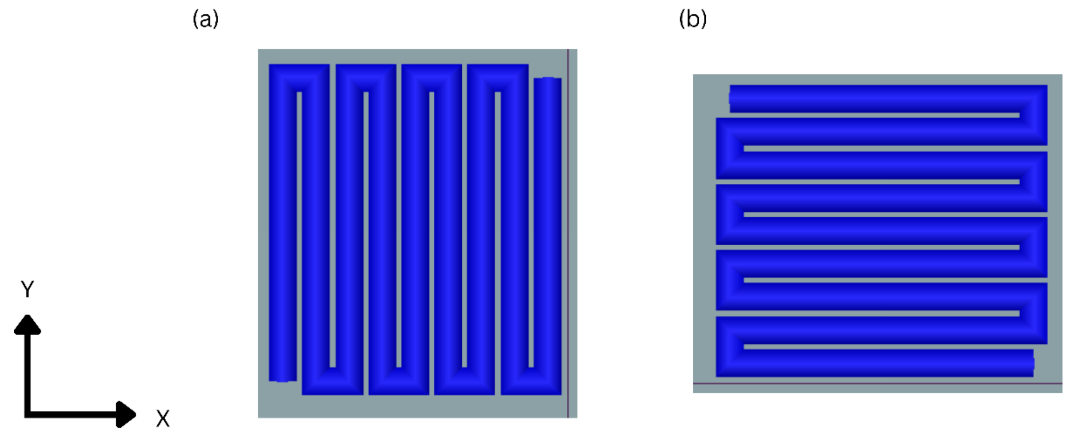

Figure 5: Print path for (a) uni- and bi-directional compression specimen (a)+(b)

In contrast, the bi-directional print strategy alternated the filament deposition direction between layers. Specifically, the first layer was printed unidirectionally along the Y-axis (like Figure 5 (a)), while the subsequent layer was printed along the X-axis (as shown in Figure 5 (b)). This alternating print direction was repeated for all 13 layers to create a woven-like structure intended to increase interlayer bonding and reduce anisotropic mechanical behavior. A schematic of the print path for the combined bi-directional print is shown in the figure below.

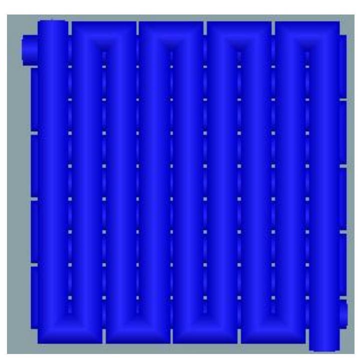

Figure 6: Print path for combined bi-directional compression specimen

Compression testing was performed in both the X and Y directions to assess the effect of print orientation on mechanical performance. Testing in the Y-direction corresponds to loading the sample along the same direction as the Y-axis (vertical relative to the print pattern), while X-direction testing corresponds to loading along the X-axis (horizontal relative to the print pattern), as indicated by the coordinate system in Figure 5.

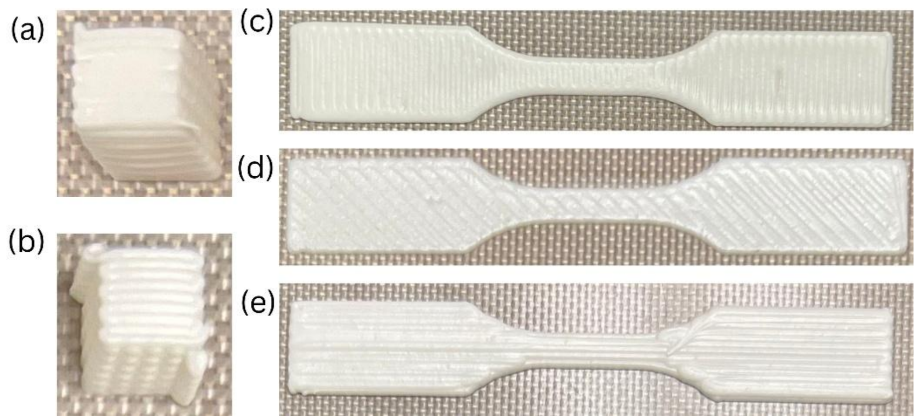

Figure 7: Printed specimen: (a) uni-directional cube, (b) bi-directional cube, (c) 90-degree dogbone, (d) 45-degree dogbone, (e) 0-degree dogbone

In addition to compression specimens, dogbone samples for tensile testing were printed in three orientations: 0°, 45°, and 90° relative to the loading axis as shown in Figure 7. The 0° print direction corresponds to filament deposition along the length of the dogbone specimen, while the 90° print direction corresponds to deposition perpendicular to the length of the dogbone. The 45° print orientation involved filament deposition at a 45° angle relative to the loading direction. Representative images of each print orientation for the dogbone specimens are provided in subsequent figures for clarity.

These print strategies were implemented to systematically study the effect of filament alignment and print architecture on the anisotropic mechanical response of 3D printed epoxy syntactic foams.

2.5 Chapter Conclusion

In this chapter, the development and processing of 3D printable epoxy syntactic foam inks suitable for Direct Ink Writing (DIW) were detailed. The inks were formulated using EPON^{TM} 815C epoxy, hollow glass microballoons of varying densities and sizes, fumed silica, and a thixotropic additive to tailor rheological behavior for printability. Rheological characterization confirmed desirable shear-thinning behavior and sufficient yield stress for shape retention during printing.

A custom-built DIW printer was used for specimen fabrication, with standardized printing parameters such as a 410 µm nozzle size, 10 mm/min print speed, and controlled pneumatic pressures ranging from 3 to 13 psi. Print strategies involving unidirectional and bidirectional architectures were implemented to study the effects of filament orientation and anisotropy on mechanical performance. The procedures developed in this chapter provided a robust framework for fabricating consistent, structurally stable specimens for subsequent mechanical characterization, discussed in the following chapters.

Chapter 3: Mechanical Properties Characterization

3.1 Introduction

Mechanical characterization of epoxy syntactic foams is essential to evaluate their suitability for lightweight structural applications. The mechanical performance of syntactic foams is highly dependent on their constituent materials, microstructure, and processing methods. In this study, both cast and 3D printed dogbone specimens were fabricated to compare the mechanical performance of the two fabrication methods. Casted specimens were prepared by pouring the mixed epoxy syntactic foam ink into silicone molds conforming to ASTM D638 Type V geometry. However, due to the high viscosity of the formulated inks resulting from the addition of glass microballoons and rheological modifiers, casting posed several challenges. The limited flowability of the material often led to incomplete mold filling, entrapped air, and void formation within the samples, which could potentially reduce the mechanical performance of the casted specimens due to stress concentrations and premature failure. In contrast, Direct Ink Writing (DIW) 3D printing offers a layer-by-layer material deposition approach that enables precise control over the geometry and architecture of the printed parts. However, DIW introduces additional factors such as print orientation and anisotropy, which can significantly influence the mechanical response of the printed syntactic foam structures [15].

This chapter presents a detailed investigation into the mechanical properties of DIW 3D printed epoxy syntactic foams formulated with three different types of glass microballoons (GMBs): S60, iM16K, and iM30K. Each GMB type exhibits distinct particle sizes, wall thicknesses, and crush strengths, which directly influence the tensile and compressive behavior of the resulting composite [16, 17]. Furthermore, the effect of print orientation on mechanical performance is explored through tensile testing of samples printed in 0°, 45°, and 90° directions for tensile properties. Anisotropy due to print directionality is examined by testing compression cubes in both the X and Y loading directions for uni- and bi-directional printed specimens.

To further enhance the mechanical performance beyond the base ink formulations, hybrid inks consisting of varying weight ratios of iM16K and iM30K GMBs were developed. The hybrid ink approach aims to leverage the desirable characteristics of both GMB types by combining the low density of iM16K with the superior strength of iM30K to create a 3D printable ink for fabricating syntactic foam with optimized specific strength and modulus. Tensile and compressive tests were conducted on the hybrid ink samples to assess their performance relative to the base inks.

In addition to the traditional tensile and compressive properties, crashworthiness parameters including energy absorption (EA), specific energy absorption (SEA), maximum compressive force (MCF), peak compressive force (PCF), and crush force efficiency (CFE) were calculated for all hybrid ink samples. These parameters provide critical insight into the energy dissipation capability and structural efficiency of the syntactic foams, which are important metrics for applications requiring impact mitigation or energy absorption [18].

The results presented in this chapter establish a comprehensive understanding of how GMB type, print orientation, and hybrid ink formulation influence the mechanical properties of DIW 3D printed epoxy syntactic foams. This forms the foundation for selecting the optimal material system for further structural evaluation, as discussed in Chapter 4.

3.2 Tensile Properties Characterization

All tensile tests were conducted using an Instron universal testing system equipped with a 5 kN load cell and wedge grips to securely hold the specimens during loading. The testing procedure was carried out at a constant crosshead displacement rate of 1 mm/min, following standard practices for polymer composite materials. The primary tensile properties measured were tensile strength, tensile modulus, and failure strain, which provide key insights into the load-bearing capability, stiffness, and ductility of the developed materials.

Tensile Stress and Strain were calculated using the following equations:

$$\sigma = \frac{W}{A_0} \qquad \text{Eq. 4}$$

$$\epsilon = \frac{\Delta L}{L_0} \qquad \text{Eq. 5}$$

Where σ is tensile stress (engineering), W is Load, A_0 is the original cross-sectional area, and ε is strain, ΔL is elongation and L_0 is the original distance between the gage marks.

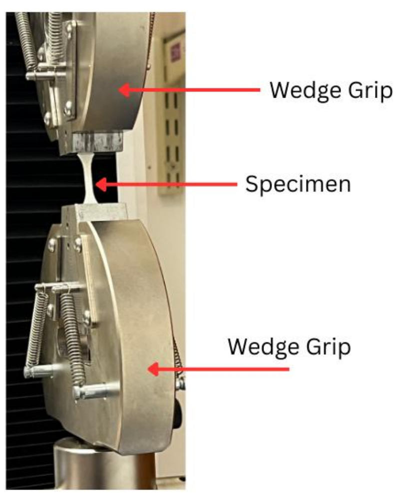

Figure 8: Tensile Testing Experimental Set-Up

3.2.1 Base Inks Tensile Properties

The tensile test results for the casted base inks are illustrated in Figure 9 below. Figures 9 (a)-(c) show the tensile stress versus tensile strain response for the casted S60, iM16K, and iM30K specimens, respectively. Each plot represents three replicate samples tested for each formulation. On average, the iM30K cast specimens exhibited the highest stiffness with a tensile modulus of 0.674 GPa, compared to 0.577 GPa for iM16K and 0.598 GPa for S60. This is reflected by the steeper initial slope of the stress-strain curves shown in Figures 9 (a)-(c). In addition to its higher stiffness, the iM30K cast specimens also demonstrated the highest tensile strength among the three casted formulations and failed at larger strains, achieving an average tensile strength of 33.58 MPa, compared to 28.74 MPa for iM16K and 27.50 MPa for S60. This superior mechanical performance of the iM30K specimens is attributed to several factors, including the smaller particle size and higher crush strength of the iM30K glass microballoons, which contribute to a denser and more reinforcing microstructure. Moreover, the lower volume fraction of iM30K microballoons relative to iM16K due to its higher true density promotes greater epoxy matrix continuity, while its higher density relative to S60 microballoons reduces stress concentrations and enhances load transfer efficiency. A similar trend was reported by Gupta and Nagorny where they found tensile strength increased with microballoon density [4]. However, despite the improved mechanical performance, considerable variability was observed across the casted specimens, as shown in Figures 9 (d) and (e), which summarize the tensile modulus and tensile strength with error bars representing standard deviation. This variability is likely due to inherent challenges associated with casting highly viscous syntactic foam inks, where limited flowability can result in void formation and poor particle dispersion, ultimately leading to reduced and inconsistent mechanical performance.

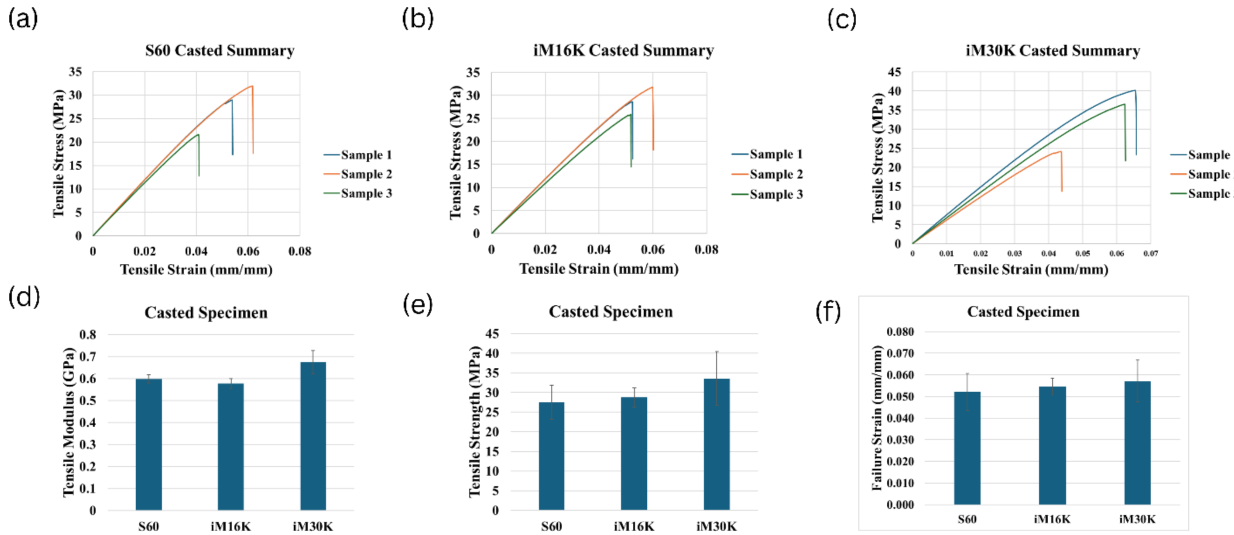

Figure 9: Tensile Test Results for Casted Base Inks for: (a) S60, (b) iM16K, (c) iM30K, (d) Tensile Modulus Comparison, (e) Tensile Strength Comparison, (f) Failure Strain Comparison

The figure below shows the schematic of the dogbone specimen and the corresponding SEM images of the fracture surface after tensile testing. As shown in Figure 10 (a), the region of interest for SEM imaging was taken at the cross-section of the fracture surface in the gauge section of the tensile specimen. Figures 10 (b) and (c) display the SEM images at different magnifications, revealing the microstructural features of the epoxy syntactic foam. The glass microballoons appear to be relatively well distributed throughout the cross-section of the specimen, indicating good dispersion during the ink mixing and printing process. However, the presence of voids and defects can also be observed within the matrix, likely resulting from air entrapment during ink preparation or the casting process. These voids can serve as stress concentrators, potentially leading to premature failure or reduced mechanical performance, particularly in casted specimens where flowability limitations make void formation more prominent.

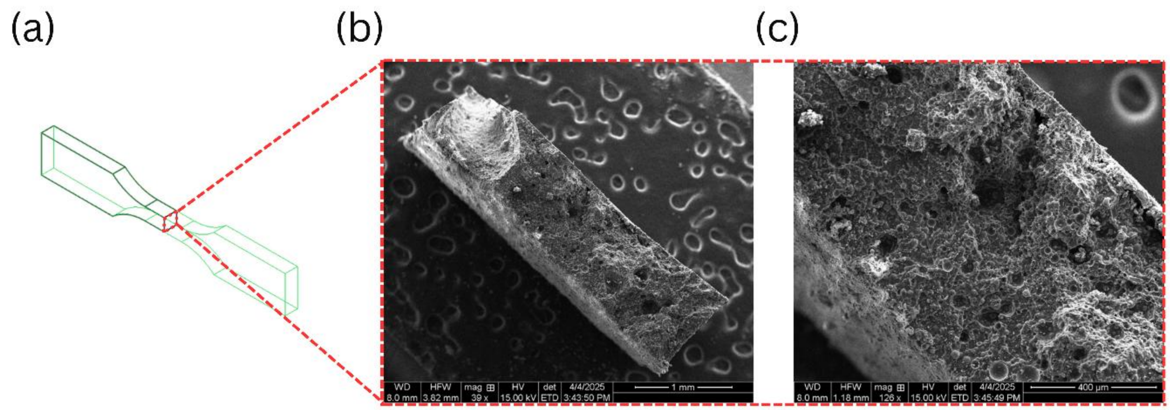

Figure 10: schematic of the dogbone specimen and the corresponding SEM images of the fracture surface after tensile testing (a) lower magnification, (b) higher magnification

Furthermore, the SEM images in Figure 10 reveal good interfacial bonding between the epoxy matrix and the glass microballoons. There is minimal evidence of microsphere pull-out or interfacial debonding across the fracture surface, suggesting that the adhesion between the matrix and the microballoons was sufficient to promote effective load transfer during tensile loading. This strong interfacial bonding likely contributed to the overall mechanical performance of the material, as failure predominantly occurred through fracture of the matrix and crushing of the microballoons rather than interfacial separation. The presence of fracture surfaces displaying broken microspheres embedded within the matrix further supports the observation of good matrix-microballoon adhesion.

Figure 11 below shows the tensile stress versus strain plots for the 3D printed samples fabricated using the base ink formulations of S60, iM16K, and iM30K. Figures 11 (a)-(c) correspond to the S60 ink printed in the 0°, 45°, and 90° orientations, respectively. Figures 11 (d)-(f) represent the iM16K ink, while Figures 11 (g)-(i) show the results for the iM30K ink across the same print orientations. Each plot presents the tensile response of three replicate samples for each condition. Like the cast samples, the tensile properties for the 3D printed specimens were characterized based on tensile strength, tensile modulus, and failure strain.

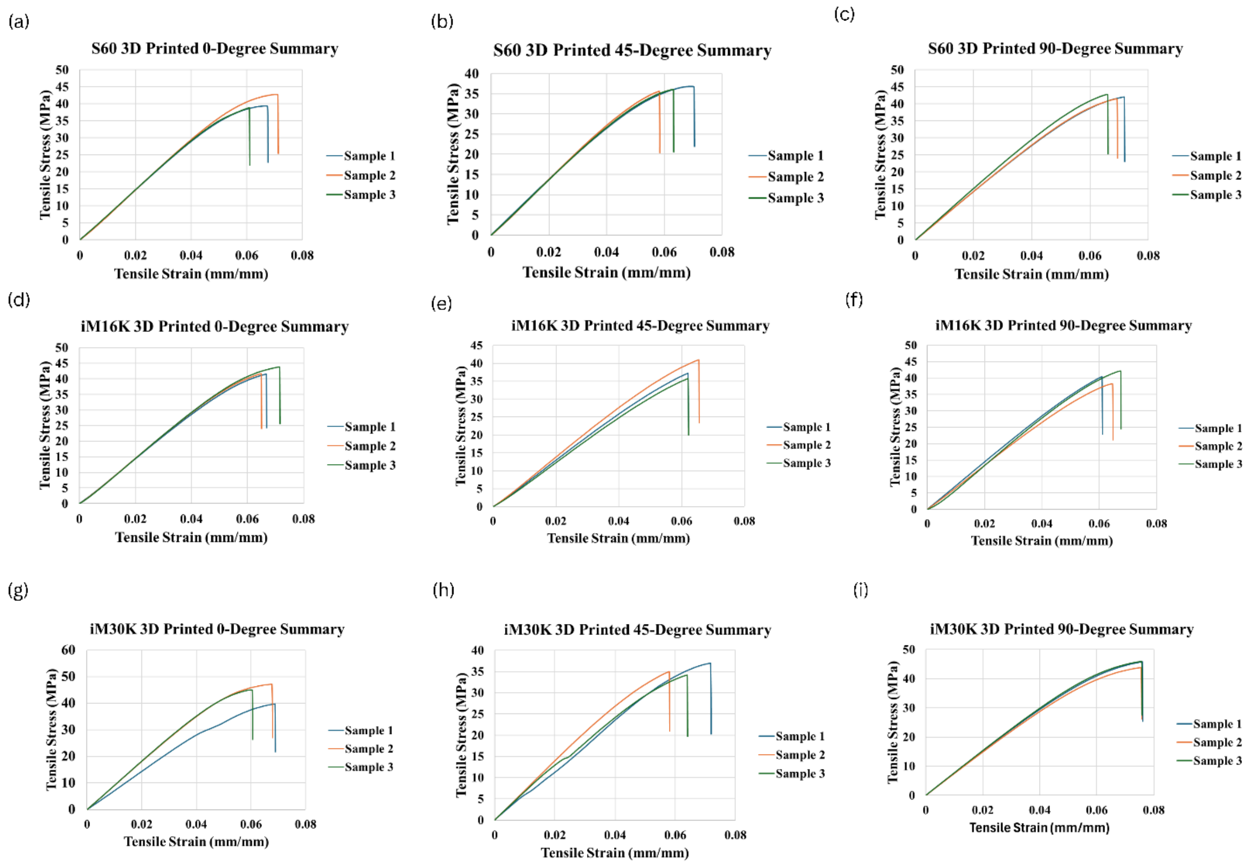

Figure 11: Tensile stress versus strain plots for the 3D printed samples fabricated using the base ink formulations of S60, iM16K, and iM30K

Figure 12 shows a clear trend where the 0° printed specimens consistently exhibited the highest tensile modulus across all three inks. This behavior is attributed to the loading direction being aligned along the continuous extruded filament paths in the 0° orientation, which maximizes stiffness due to minimal inter-layer effects and full utilization of the filament's inherent properties. In terms of tensile strength, the 0° printed specimens generally showed the highest values or were comparable to the 90° printed specimens, depending on the ink type. The strength of the 0° orientation is similarly driven by the continuous filament alignment with the loading direction, resulting in efficient load transfer and reduced susceptibility to interlayer failure [19].

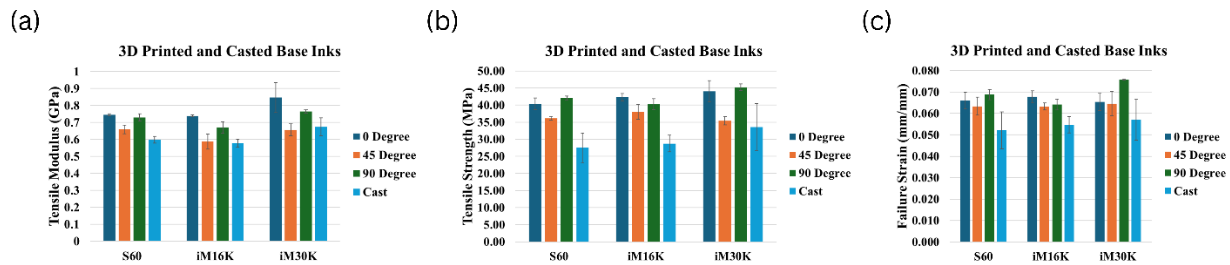

Figure 12: Comparison of (a) Tensile Modulus, (b) Tensile Strength and (c) Failure Strain for 3D Printed and Casted Base Inks

In contrast, the 45° printed specimens exhibited the lowest tensile modulus and tensile strength across all base inks. This reduction in mechanical performance is expected, as the 45° orientation introduces a highly shear-dominated loading path along the filament interfaces. In this configuration, the load is not carried directly along the filaments but is instead transferred through interlayer bonding and matrix deformation, making the specimens more prone to delamination and sliding between layers. The iM30K ink consistently demonstrated the highest tensile performance for all print orientations, owing to its smaller microsphere size, higher crush strength, and lower volume fraction of microspheres relative to iM16K, which promotes better matrix continuity and load-bearing capability. Furthermore, across all three base ink formulations (S60, iM16K, and iM30K), the casted specimens consistently underperformed compared to their 3D printed counterparts in terms of tensile modulus (a), tensile strength (b), and failure strain (c). This trend is likely due to a higher concentration of voids and entrapped air in the cast specimens, which act as stress concentrators and reduce overall mechanical performance compared to the more densely packed and homogenized structure achieved through DIW 3D printing.

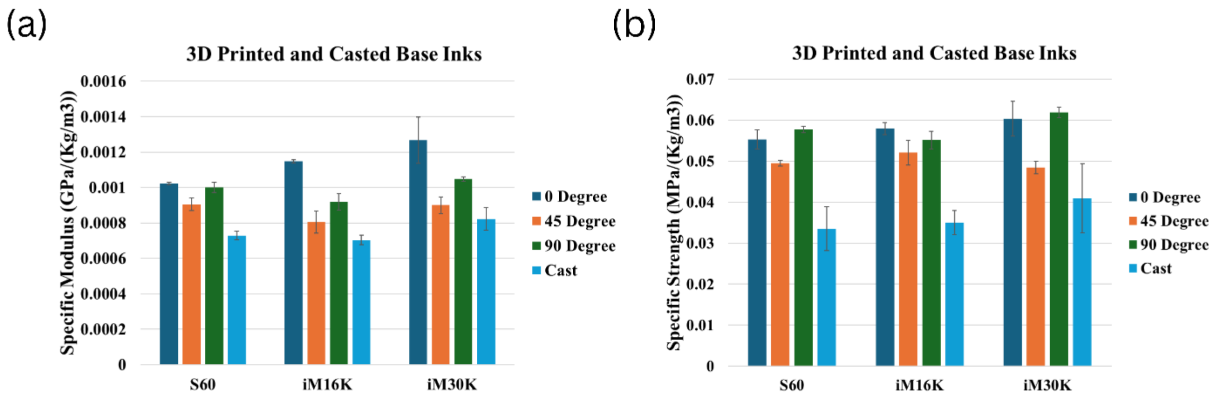

Figure 13: Comparison of (a) Specific Tensile Modulus, (b) Specific Tensile Strength for 3D Printed and Casted Base Inks

Figure 13 presents the specific modulus (a) and specific strength (b) of 3D printed and casted specimens for S60, iM16K, and iM30K inks. The 0° printed specimens consistently exhibited the highest specific modulus across all inks, indicating superior stiffness due to filament alignment with the loading direction, which enables more efficient stress transfer along the axis of applied force. The iM30K ink achieved the highest specific strength and specific modulus across all print orientations, reflecting its enhanced load-bearing capacity and the mechanical benefits conferred by its smaller, stronger microballoons. In contrast, the 45° printed specimens demonstrated the lowest performance overall, which can be attributed to shear-dominated loading and weaker interlayer bonding at this print angle, leading to early failure. Among the casted samples, the iM30K formulation again outperformed the other inks, achieving the highest specific tensile modulus (8.88×10^{-4} GPa/(kg/m^3)) and specific strength (4.42×10^{-2} MPa/(kg/m^3)), underscoring the inherent material advantages of the iM30K ink, even in the absence of directional reinforcement provided by the DIW process.

Figure 14 below shows SEM images of the cross-section and fracture surfaces of representative 3D printed tensile specimens printed in the 0°, 45°, and 90° orientations using the base iM30K ink. For each print orientation, images are provided for (a, d, g) the cross-section of the specimen, (b, e, h) the untested surface of the cross-section, and (c, f, i) the fracture surface after tensile testing.

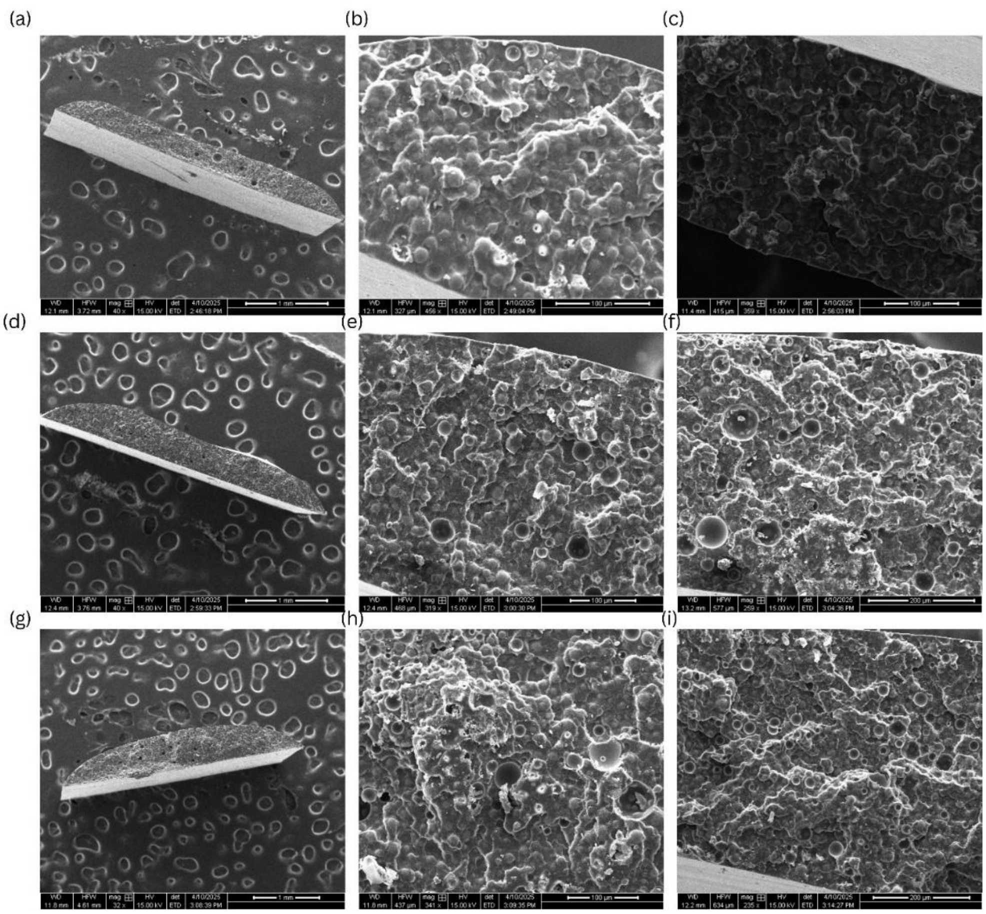

Figure 14: SEM images of the cross-section and fracture surfaces of representative 3D printed tensile specimens printed in the 0°, 45°, and 90° orientations using the base iM30K ink

The SEM images reveal several key microstructural characteristics of the 3D printed epoxy syntactic foam specimens across all print orientations. Firstly, the distribution of glass microballoons is observed to be relatively uniform throughout the cross-section for all three print orientations (Figures 14 (a), (d), (g)). This indicates effective mixing of the ink prior to printing and successful extrusion without significant particle agglomeration or settling. The cross-sections also exhibit a well-defined and nearly rectilinear geometry, with only slight curvature at the specimen edges, likely due to surface tension effects during the printing process. This demonstrates good dimensional control and shape retention during the DIW printing process.

Additionally, the presence of some voids and defects within the matrix can be seen in the higher magnification images (Figures 14 (b), (e), (h)), which are likely attributed to air entrapment during ink preparation or small gaps formed during filament deposition. However, these voids are relatively sparse and isolated, suggesting that they are unlikely to dominate the mechanical response of the material.

Importantly, no obvious signs of weak interlayer bonding or distinct print lines are visible across the cross-sections and fracture surfaces for any of the print orientations. The interface between adjacent deposited filaments appears well-fused, with continuous epoxy matrix bridging across layers. This observation is critical for the mechanical performance of DIW printed materials, as poor interlayer bonding or lack of fusion between print lines would serve as preferential sites for crack initiation and delamination under tensile loading [20]. The absence of such defects suggests that the printing parameters and ink rheology were optimized to promote sufficient interdiffusion and bonding between layers, leading to enhanced mechanical integrity of the printed parts. The fracture surfaces (Figures 14 (c), (f), (i)) further confirm this, as failure appears to propagate through the matrix and microballoons rather than along layer boundaries, indicating bulk-like failure behavior rather than delamination-driven failure.

Additionally, it must be noted that the cross-sectional area used in the tensile stress-strain measurements were measured using a pair of vernier calipers for the width and a micrometer screw gauge for the thickness. This essentially assumed the cross-sectional area of the tensile specimen were rectilinear in shape, however, the morphology seen in the SEM images in Figure 14 confirms the curvature on the edges of the cross-sectional area, thus reducing the overall area of the specimen. As a result, to obtain an idea about how far the strength values were underestimated, a correction factor (CF) for a small selection of specimen was used as follows:

$$CF = \frac{A_0}{A} \qquad \text{Eq. 6}$$

Where A_0 is the originally measured cross-sectional area and A is the true cross-sectional area, obtained from image processing through the usage of ImageJ software. The results of the example specimen are shown in the table below:

Table 3: Corrected strength using an area correction factor

Orientation	ImageJ Area (mm^2)	A_0/A	Original Strength (MPa)	Corrected Strength (MPa)
0°	1.15	1.73	42.33	73.23
45°	1.30	1.81	38.00	68.78
90°	1.41	2.40	40.23	96.55

Following the application of the area correction factor, the true tensile strength values showed significant increases across all orientations. For the 0° specimen, the corrected strength rose from 42.33 MPa to 73.23 MPa, representing an increase of approximately 73%. The 45° specimen's strength increased from 38.00 MPa to 68.78 MPa, which is about an 81% improvement. Most notably, the 90° specimen exhibited the largest relative increase, with the corrected strength rising from 40.23 MPa to 96.55 MPa—an enhancement of approximately 140%. These substantial increases highlight how conventional measurement techniques can significantly underestimate the true strength of specimens with curved or non-rectilinear cross sections, reinforcing the importance of image-based area correction for accurate mechanical property evaluation.

3.2.2 Hybrid Inks Tensile Properties

Figure 15 below shows the tensile stress versus strain plots for the 3D printed specimens fabricated using the hybrid ink formulations consisting of varying weight ratios of iM30K and iM16K glass microballoons. The first row of plots, Figures 15 (a)-(c), correspond to the 30K_1 16K_3 hybrid ink, printed in the 0°, 45°, and 90° orientations respectively, with three replicate samples shown for each condition. Figures 15 (d)-(f) represent the 30K_2 16K_2 hybrid ink, printed in the 0°, 45°, and 90° orientations. Finally, Figures 15 (g)-(i) show the results for the 30K_3 16K_1 hybrid ink across the same print orientations. Like the base ink specimens, tensile testing was conducted to evaluate the tensile strength, tensile modulus, and failure strain of the hybrid inks, while also assessing the influence of print orientation on the tensile response. The primary focus of this section is to evaluate how varying amounts of iM16K and iM30K glass microballoons within the hybrid ink formulations influence the tensile behavior of the printed specimens, with particular attention paid to identifying trends in stiffness, strength, and anisotropy across the different hybrid ratios.

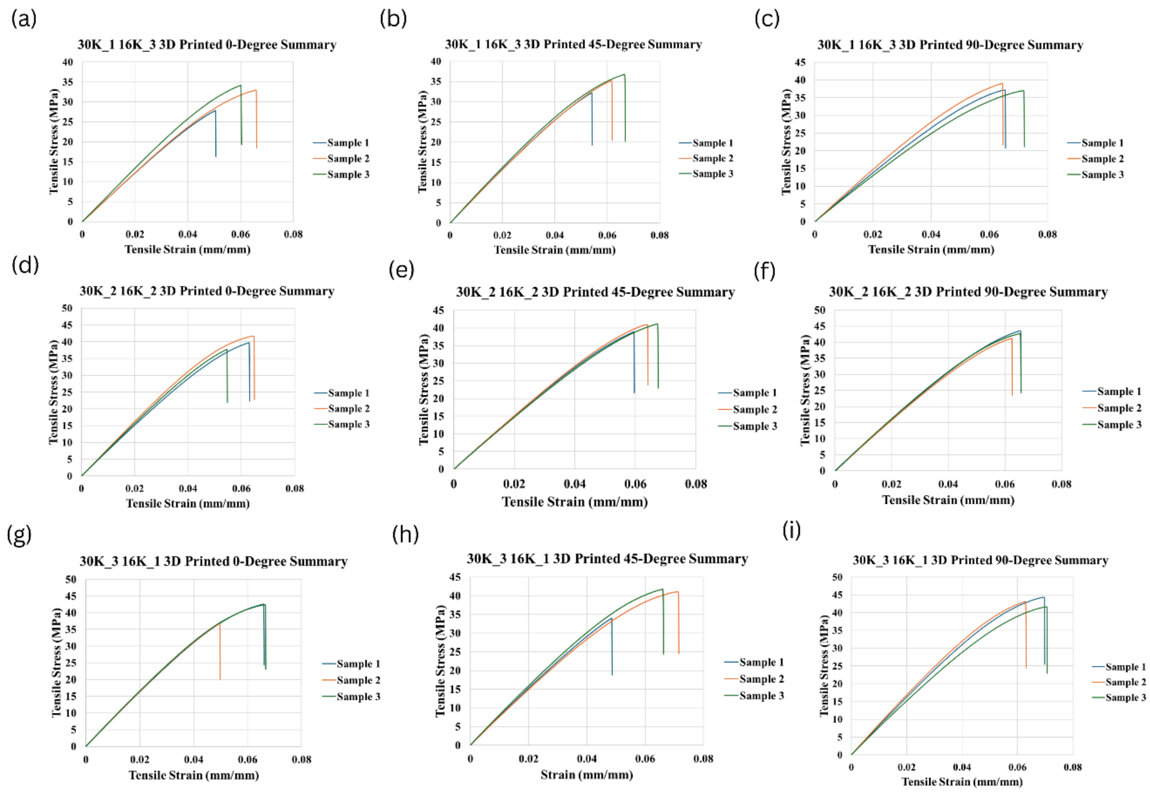

Figure 15: tensile stress versus strain plots for the 3D printed specimens fabricated using the hybrid ink formulations consisting of varying weight ratios of iM30K and iM16K glass microballoons

Figure 16 below summarizes the tensile modulus, tensile strength, and failure strain of the 3D printed hybrid ink specimens for all three hybrid formulations (30K_1 16K_3, 30K_2 16K_2, and 30K_3 16K_1) tested in the 0°, 45°, and 90° print orientations.

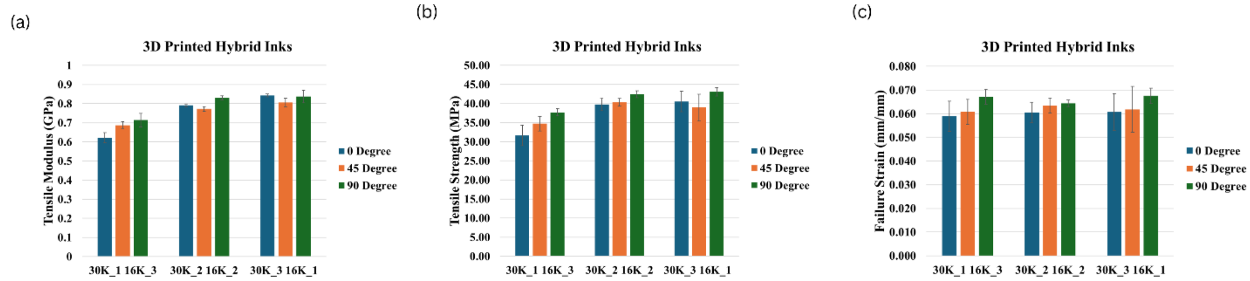

Figure 16: Comparison of (a) Tensile Modulus, (b) Tensile Strength, and (c) Failure Strain of the 3D printed hybrid ink specimens

As shown in Figures 16 (a)-(c), increasing the content of iM30K glass microballoons in the hybrid formulation resulted in noticeable improvements in both tensile modulus and tensile strength across all print orientations. The 30K_3 16K_1 hybrid ink exhibited the highest tensile modulus, reaching an average value of 0.842 GPa in the 0° orientation, compared to 0.791 GPa for the 30K_2 16K_2 ink and 0.621 GPa for the 30K_1 16K_3 ink. This trend is consistent with expectations, as the higher density and smaller size of iM30K microspheres contribute to greater matrix continuity and improved load transfer within the printed structure.

A similar trend was observed for tensile strength, where the 30K_3 16K_1 hybrid ink achieved the highest average tensile strength of 43.05 MPa in the 90° orientation, while the 30K_2 16K_2 and 30K_1 16K_3 inks exhibited average strengths of 42.45 MPa and 37.70 MPa, respectively. Interestingly, the 0° print orientation, which would traditionally be expected to exhibit the highest tensile strength due to filament alignment along the loading direction, did not consistently outperform the other print orientations across all hybrid inks. This behavior is likely attributed to the increased sensitivity of the 0° printed specimens to defects along the continuous filament path. In the 0° orientation, the applied load is directly carried by individual extruded filaments; therefore, any localized defects such as voids, air entrapment, surface irregularities, or inconsistencies during extrusion can act as critical stress concentrators. These defects can initiate early failure along the print line, reducing the overall tensile strength. In contrast, the 45° and 90° orientations involve load transfer across multiple filament interfaces, which may help redistribute stress and limit the impact of localized defects. The relatively higher tensile strength observed in the 45° printed specimens compared to the 90° orientation may also suggest that the angled filament arrangement in the 45° print provides a more tortuous crack path, delaying failure despite the reliance on interlayer bonding. Overall, these results highlight that print quality and defect sensitivity play a critical role in determining the tensile performance of DIW printed syntactic foams, particularly for specimens printed in the 0° orientation.

Furthermore, the failure strain remained relatively consistent across all hybrid inks and print orientations, with values ranging from 0.059 to 0.068 mm/mm. The 30K_3 16K_1 hybrid ink exhibited slightly higher failure strains in the 90° orientation, reaching a maximum of 0.067 mm/mm, indicating that increasing iM30K content did not significantly compromise the ductility of the printed material.

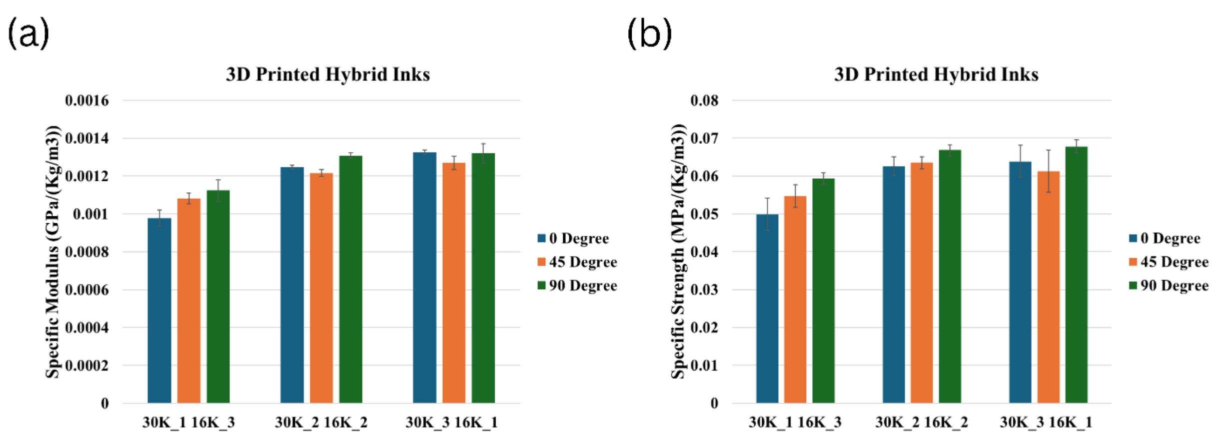

Figure 17: Comparison of (a) Specific Tensile Modulus, (b) Specific Tensile Strength of the 3D printed hybrid ink specimens

Figure 17 shows the specific modulus (a) and specific strength (b) of three 3D printed hybrid ink formulations—30K_1:16K_3, 30K_2:16K_2, and 30K_3:16K_1—tested in 0°, 45°, and 90° print orientations. The middle formulation (30K_2:16K_2) and the rightmost formulation (30K_3:16K_1) consistently outperformed the leftmost formulation (30K_1:16K_3) in both specific modulus and specific strength across all orientations. This trend suggests that higher proportions of iM30K microballoons (either through increased weight fraction or higher stiffness contribution) improve the structural efficiency of the printed parts, likely due to increased reinforcement and enhanced packing density. Additionally, the superior performance of the middle and right formulations indicates a more effective balance between the high strength of iM30K and the lightweight character of iM16K, leading to optimized stiffness-to-weight and strength-to-weight ratios for DIW applications. Based on these findings, the 30K_2:16K_2 and 30K_3:16K_1 formulations stand out as the most promising candidates for printing lightweight honeycomb structures, offering an optimal combination of mechanical performance and material efficiency.

3.3 Compression Properties Characterization

All compression tests were conducted using an Instron universal testing system equipped with a 5 kN load cell and compression platens to apply uniform loading to the specimens. The testing procedure was carried out at a constant crosshead displacement rate of 1 mm/min, following standard practices for polymer composite materials. The primary compressive properties measured were peak compressive strength and compressive modulus, which provide key insights into the load-bearing capability, stiffness, and resistance to deformation of the developed materials under compressive loading conditions.

Compressive Stress and Strain were calculated using the following equations:

$$\sigma = \frac{W}{A_0} \qquad \text{Eq. 7}$$

$$\epsilon = \frac{\Delta H}{H_0} \qquad \text{Eq. 8}$$

Where σ is compressive stress (engineering), W is Load, A_0 is the original cross-sectional area, and ε is strain, ΔH is displacement and H_0 is the original height of the specimen.

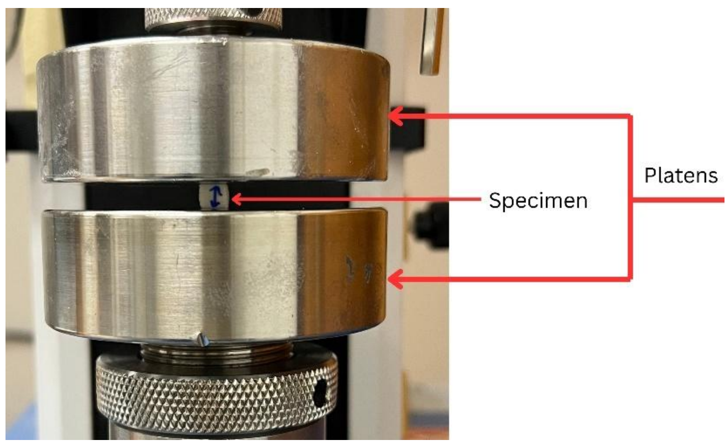

Figure 18: Compression Test Experimental Set-Up

3.3.1 Base Inks Compressive Properties

Figure 19 below shows the compressive stress versus strain curves for the casted specimens of the base inks: S60, iM16K, and iM30K. While the general compressive response follows the expected behavior of syntactic foams with an initial linear elastic region, a plateau associated with microsphere crushing, and final densification the results exhibit significant variability between samples. This inconsistency is largely attributed to defects introduced during the casting process, particularly for highly viscous inks containing a high-volume fraction of glass microballoons. The limited flowability of these materials during casting can lead to poor mold filling, air entrapment, and void formation, which act as stress concentrators and reduce the overall compressive performance of the specimens.

Interestingly, although certain cast specimens reached compressive strengths exceeding 60 MPa, which is higher than the peak compressive strength observed for all 3D printed specimens (which remained below 50 MPa), this behavior aligns with the expectation that casted samples in an ideal, defect-free condition should outperform 3D printed samples due to the absence of interlayer interfaces and print-induced anisotropy. However, the large variability in the cast results highlights the difficulty of achieving consistent mechanical performance when casting highly viscous syntactic foam materials. These results further reinforce the significance and advantage of DIW 3D printing, which allows for better geometric control, more uniform material distribution, and reduced void content, leading to improved repeatability and reliability in mechanical performance.

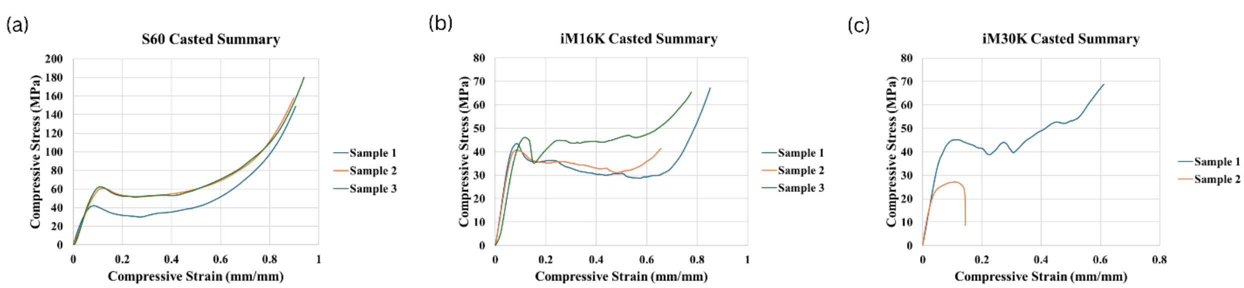

Figure 19:Ccompressive stress versus strain curves for the casted specimens of the base inks: (a) S60, (b) iM16K, and (c) iM30K

Figure 20 below shows the compressive stress versus strain curves for the 3D printed base ink specimens tested in compression for all three inks (S60, iM16K, and iM30K). For each ink, compression testing was performed in four different configurations: X-direction and Y-direction for unidirectional prints and bidirectional prints. Figures 20 (a)-(d) correspond to the S60 ink, Figures 20 (e)-(h) correspond to the iM16K ink, and Figures 20 (i)-(l) correspond to the iM30K ink. Each plot shows three replicate samples for each print configuration. The compressive response for all inks generally followed an initial linear elastic region, followed by a plateau region associated with microsphere crushing and matrix deformation, and finally densification at higher strains. The key compressive properties extracted from these curves include the compressive modulus, peak compressive strength, and strain at peak stress.

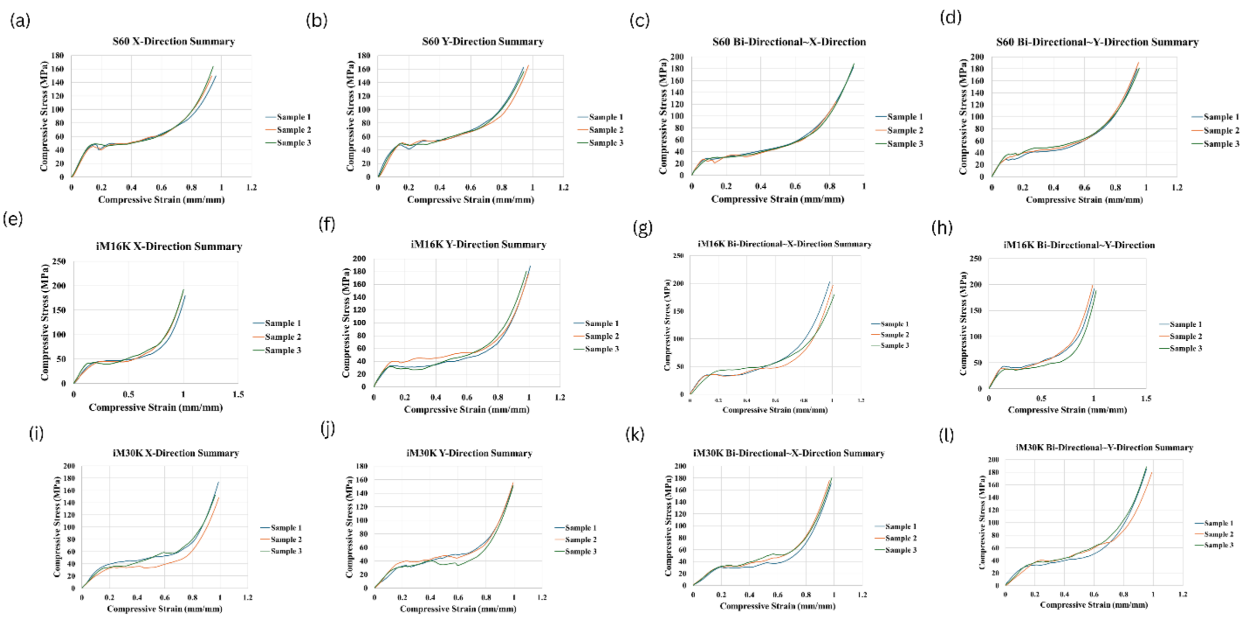

Figure 20: Compressive stress versus strain curves for the 3D printed base ink specimens tested in compression for all three inks (S60, iM16K, and iM30K)

Figure 21 below summarizes the average compressive modulus, peak compressive strength, and strain at peak stress for all base inks tested in each print configuration. A clear trend is observed where the S60 ink exhibited the highest compressive modulus, particularly in the Bi-X and a relatively high value in the Bi-Y directions, with values reaching 0.619 GPa. This is likely due to the larger size and thicker walls of the S60 microspheres, which provide greater stiffness under compressive loading. However, despite the higher stiffness, the S60 ink also exhibited the lowest strain at peak stress, with values as low as 0.104 mm/mm, indicating a more brittle behavior under compression.

In contrast, the iM16K and iM30K inks exhibited lower compressive modulus values, ranging from 0.236 GPa to 0.590 GPa depending on the print direction, but generally demonstrated higher strain at peak stress, with some configurations reaching values of 0.245 mm/mm. The peak compressive strength for all inks was relatively comparable, generally falling within the range of 28.68 MPa to 49.21 MPa, although the S60 ink in the X and Y directions exhibited slightly higher strengths compared to the other inks.

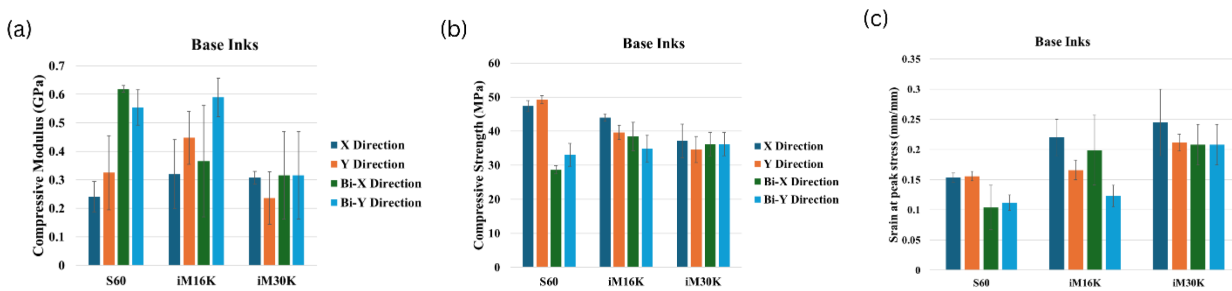

Figure 21:Compressive modulus, peak compressive strength, and strain at peak stress for all base inks tested in each print configuration

It is important to note the wide variation in strain at peak stress observed across different inks and print directions, as indicated by the large error bars in Figure 21 (c). This variability may be attributed to factors such as localized defects, variation in microsphere distribution, and the inherent differences in energy absorption capability between unidirectional and bidirectional printed samples. Overall, these results highlight the influence of both ink formulation and print direction on the compressive response of the printed syntactic foam specimens.

3.3.1 Hybrid Inks Compressive Properties

Figure 22 below shows the compressive stress versus strain curves for the 3D printed hybrid ink specimens tested in compression. Three different hybrid formulations were evaluated based on varying weight ratios of iM30K to iM16K glass microballoons: iM30K_1 iM16K_3, iM30K_2 iM16K_2, and iM30K_3 iM16K_1. For each hybrid formulation, compression testing was conducted in four configurations — X-direction, Y-direction for unidirectional prints, and for bidirectional prints. Figures 22 (a)-(d) correspond to the iM30K_1 iM16K_3 ink, Figures 22 (e)-(h) correspond to the iM30K_2 iM16K_2 ink, and Figures 22 (i)-(l) correspond to the iM30K_3 iM16K_1 ink. Each plot presents the compressive response of three replicate samples for each configuration. Similar to the base inks, the hybrid inks exhibited the characteristic compressive behavior of syntactic foams, with an initial elastic region, followed by microsphere crushing and densification at higher strains.

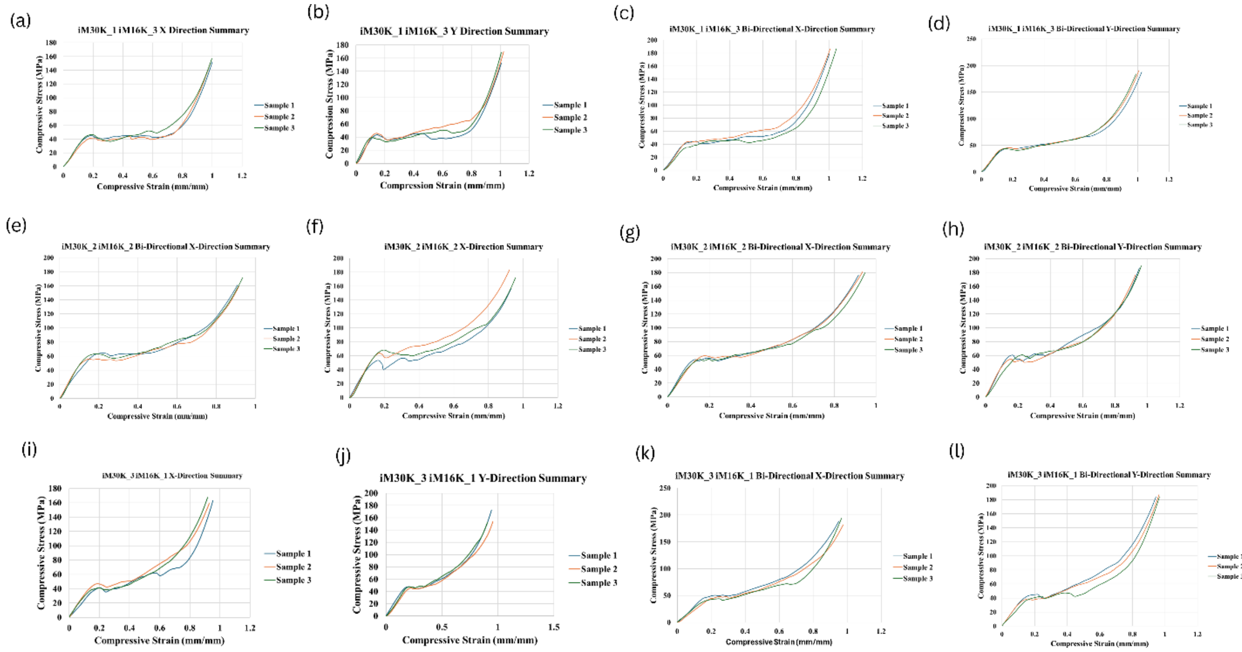

Figure 22: Compressive stress versus strain curves for the 3D printed hybrid ink specimens tested in compression

Figure 23 below summarizes the specific modulus and specific strength of each hybrid ink formulation. These properties were calculated by normalizing the average compressive modulus and peak compressive strength values by the measured density of each hybrid ink, which were 0.635 g/cm^3 for iM30K_1 iM16K_3, 0.735 g/cm^3 for iM30K_2 iM16K_2, and 0.699 g/cm^3 for iM30K_3 iM16K_1. The use of specific properties is critical in the evaluation of lightweight materials, particularly for structural applications such as energy-absorbing cores, where achieving high strength and stiffness at reduced weight is essential.

The reported specific modulus and specific strength values account for the average of all print directions tested (X, Y, Bi-X, and Bi-Y). This was done to provide a comprehensive and direction-independent assessment of each hybrid ink's mechanical performance. Such an approach is particularly important for material selection for the fabrication of hexagonal honeycomb cores, where loading directions in service may be multi-directional and not necessarily aligned with a single print orientation.

The results show that the iM30K_2 iM16K_2 hybrid ink achieved the highest specific strength, with a value of 0.081 MPa/(kg/m³), while the specific modulus exhibited greater variability between hybrid inks, ranging from 0.000352 to 0.000424 GPa/(kg/m³). The wider variation in specific modulus may be attributed to differences in microsphere distribution, local defects, and variations in interfacial bonding between the matrix and microspheres, which can have a more pronounced effect on the stiffness response [21, 22]. In contrast, the tighter variation observed in specific strength suggests that failure was more governed by the bulk properties of the material and was less sensitive to localized variations. Ultimately, these results provide critical insight for selecting the optimal hybrid ink for printing lightweight, high-performance honeycomb structures, balancing both specific strength and specific modulus.

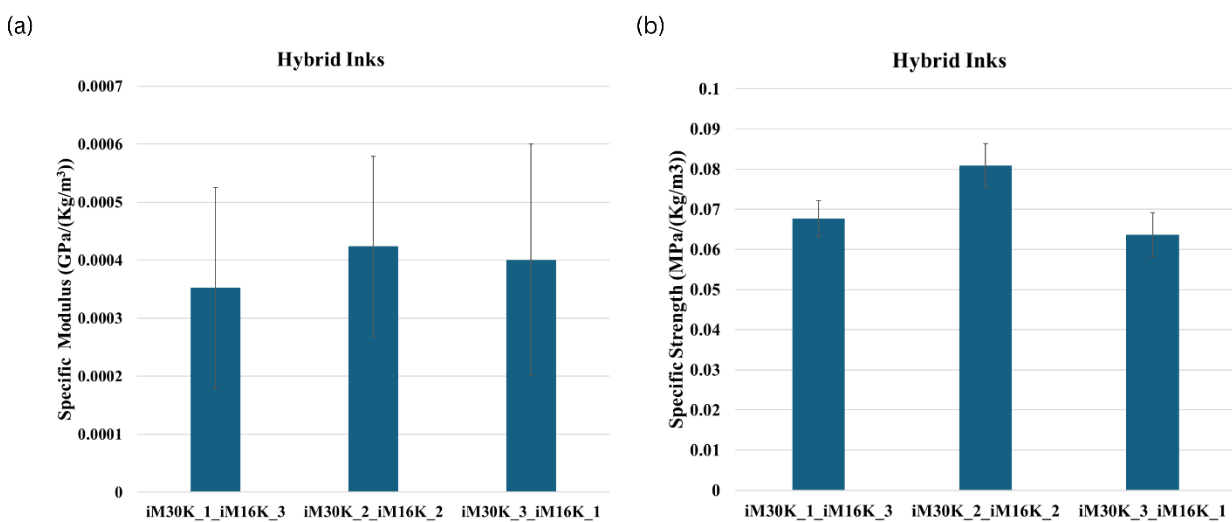

Figure 23: specific modulus and specific strength of each hybrid ink formulation

3.4 Crashworthiness Parameters of Hybrid Inks

To further evaluate the energy absorption capability and structural efficiency of the 3D printed hybrid epoxy syntactic foam specimens, several key crashworthiness parameters were calculated based on the compressive stress-strain data. These parameters provide valuable insight into the performance of lightweight materials in energy-absorbing applications, such as impact mitigation or protective structural components [23, 24]. The crashworthiness parameters considered in this study include energy absorption (EA), specific energy absorption (SEA), maximum compressive force (MCF), peak compressive force (PCF), and crush force efficiency (CFE).

Energy absorption (EA) was calculated as the area under the compressive stress-strain curve up to the densification strain limit using the following equation:

$$EA = \int_a^b F.d\delta \qquad \text{Eq. 9}$$

Specific energy absorption (SEA) was determined by normalizing the energy absorption by the mass of the specimen using the equation:

$$SEA = \frac{EA}{m} \qquad \text{Eq. 10}$$

Maximum compressive force (MCF) corresponds to the average load sustained over the plateau region of the stress-strain curve and is given by:

$$MCF = \frac{1}{\delta_b}\int_a^b F.d\delta \qquad \text{Eq. 11}$$

Peak compressive force (PCF) represents the highest load recorded during compression testing before the onset of densification.

Crush force efficiency (CFE) was calculated to evaluate the load uniformity of the material during compression and is defined as the ratio of the maximum compressive force (MCF) to the peak compressive force (PCF):

$$CFE = \frac{MCF}{PCF} \qquad \text{Eq. 12}$$

These crashworthiness parameters were calculated for all hybrid ink formulations and averaged across all print directions tested (X, Y, Bi-X, and Bi-Y) to provide a comprehensive assessment of the material behavior under compressive loading. The results of the crashworthiness evaluation for each hybrid ink formulation are shown in Figure 24 below.

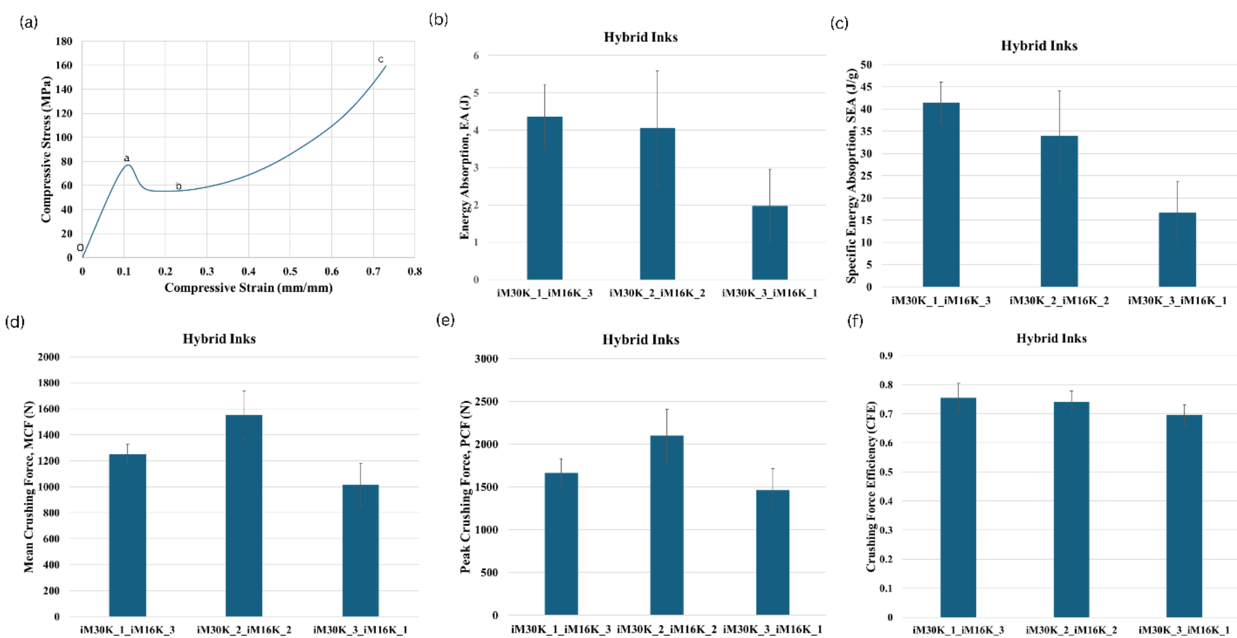

Figure 24: Crashworthiness evaluation for each hybrid ink formulation

As shown in Figures 24 (b)-(f), the iM30K_2 iM16K_2 hybrid ink demonstrated superior overall crashworthiness when compared to the other hybrid formulations. Specifically, the iM30K_2 iM16K_2 ink exhibited the highest mean crushing force (MCF) and peak crushing force (PCF), reaching values of 1551 N and 2103 N respectively, as shown in Figures 24 (d) and (e). This indicates that the iM30K_2 iM16K_2 specimens could sustain higher loads throughout the plateau region and at peak loading, suggesting enhanced energy absorption capacity and structural integrity under compressive loading.

In terms of energy absorption (EA) and specific energy absorption (SEA), while the iM30K_1 iM16K_3 hybrid ink exhibited the highest absolute EA value of 4.360 J and SEA of 41.393 J/g, the iM30K_2 iM16K_2 ink achieved values that were very comparable within 93% of the maximum recorded values as shown in Figures 24 (b) and (c). This result indicates that although iM30K_1 iM16K_3 was slightly more efficient on an energy absorption per mass basis, the iM30K_2 iM16K_2 formulation was able to combine excellent energy absorption with superior load-bearing capacity.

Coupled with the fact that the iM30K_2 iM16K_2 hybrid ink also demonstrated the highest specific strength and specific modulus, as discussed in the previous section, this hybrid formulation provides the most balanced and optimized performance across all key mechanical and crashworthiness parameters. The high specific strength ensures that the material can withstand high stresses relative to its weight, while the high specific modulus provides the necessary stiffness for load-bearing structural components. Furthermore, the superior MCF and PCF values indicate the material's ability to maintain stability and resist catastrophic failure under compressive loads.

Overall, the combination of high energy absorption capability, superior load-bearing capacity, and favorable specific properties makes the iM30K_2 iM16K_2 hybrid ink the best candidate for the fabrication of lightweight, energy-absorbing structures such as hexagonal honeycomb cores, where mechanical performance must be balanced with weight reduction for optimal efficiency in structural applications.

3.5 Chapter Conclusion

This chapter presented a comprehensive mechanical characterization of both cast and 3D printed epoxy syntactic foam specimens developed using three different base ink formulations (S60, iM16K, and iM30K) and three hybrid ink formulations with varying weight ratios of iM30K to iM16K glass microballoons. Tensile and compressive tests were performed to evaluate the influence of glass microballoon type, print orientation, and hybrid composition on the mechanical behavior of the developed materials. In addition, crashworthiness parameters were calculated for the hybrid inks to assess their energy absorption capabilities and structural efficiency for potential lightweight applications.

Tensile testing results demonstrated that the 3D printed iM30K base ink consistently exhibited the highest tensile modulus and tensile strength across all print orientations, attributed to its smaller microsphere size, higher crush strength, and lower volume fraction relative to the matrix. The 0° print orientation typically resulted in the highest tensile modulus across all inks due to loading along the filament path. However, in several cases, the 90° and 45° orientations produced comparable or higher tensile strength than the 0° orientation, likely due to defect sensitivity in the continuous extruded filament and better stress redistribution in cross-filament loading conditions.

Compressive testing results for the base inks revealed that while cast specimens exhibited higher peak compressive strengths, in some cases exceeding 60 MPa, their mechanical performance was however highly inconsistent. This variability was attributed to the presence of casting-induced defects such as voids and poor microsphere dispersion, resulting from the high viscosity of the ink formulations. In contrast, the 3D printed samples demonstrated more consistent compressive properties across all test configurations, with the S60 ink showing the highest compressive modulus due to its thicker-walled microspheres, but at the expense of lower strain at peak stress.

For the hybrid ink formulations, compressive testing further demonstrated the importance of balancing microsphere type and content. The iM30K_2 iM16K_2 hybrid ink emerged as the optimal formulation, achieving the highest specific strength and specific modulus values while also maintaining competitive energy absorption capability. Although the iM30K_1 iM16K_3 hybrid exhibited the highest energy absorption (4.360 J) and specific energy absorption (41.393 J/g), the iM30K_2 iM16K_2 hybrid closely matched these values — within 93% of the maximum EA and 82% of the maximum SEA — while demonstrating significantly higher mean crushing force (MCF) and peak crushing force (PCF). This indicated superior load-sustaining ability and structural efficiency under compressive loading, critical for energy-absorbing applications.

The crashworthiness evaluation reinforced the selection of the iM30K_2 iM16K_2 hybrid ink as the best-performing formulation, offering an optimal balance of strength, stiffness, energy absorption, and weight savings. These attributes make the iM30K_2 iM16K_2 hybrid ink the most suitable candidate for fabricating lightweight structural components, particularly for applications requiring energy absorption and impact resistance.

The following chapter focuses on the application of the optimized iM30K_2 iM16K_2 hybrid ink for the fabrication of 3D printed hexagonal honeycomb core structures. The compressive properties of the honeycomb specimens will be evaluated to validate the material's potential for use in lightweight structural and energy-absorbing applications.

Chapter 4: In-Plane Compressive Properties of Hexagonal Honeycomb Structures

4.1 Introduction

Honeycomb core structures are widely utilized in lightweight structural applications due to their high strength-to-weight ratio, excellent energy absorption capability, and efficient load distribution characteristics [25]. These cellular architectures are commonly implemented in aerospace, automotive, and marine industries, particularly as core materials in sandwich panels or energy-absorbing components [26]. The mechanical performance of honeycomb structures is highly dependent on both the material properties of the core and the geometric design parameters, such as cell size, wall thickness, and infill density [27, 28].

In this study, hexagonal honeycomb structures were fabricated using the optimized hybrid ink formulation (iM30K_2 iM16K_2) identified from previous tensile, compressive, and crashworthiness evaluations. The selection of this hybrid ink was based on its superior balance of specific strength, specific modulus, energy absorption capability, and load-bearing performance, making it an ideal candidate for the fabrication of lightweight, energy-absorbing cores.

The honeycomb structures were 3D printed using the Direct Ink Writing (DIW) process, leveraging the material and processing advantages demonstrated in earlier chapters. A 30% infill density hexagonal pattern was chosen to balance weight reduction with structural integrity. The in-plane compressive properties of the printed honeycomb specimens were investigated by performing compression testing in both the X and Y directions to assess potential anisotropy in mechanical behavior due to the honeycomb geometry and printing process.

The primary compressive properties evaluated include peak specific compressive strength, specific compressive modulus. Understanding the in-plane compressive response of the printed honeycomb structures provides critical insight into the performance of the developed epoxy syntactic foam materials in real-world structural and impact applications. The results of this chapter serve as a validation of the material development process and its potential implementation in lightweight structural core applications.

4.2 Experimental

The fabrication of the hexagonal honeycomb structures was performed using the optimized hybrid ink formulation consisting of a 50:50 weight ratio of iM30K to iM16K glass microballoons (iM30K_2 iM16K_2), identified from the mechanical characterization and crashworthiness evaluations discussed in Chapter 3. The ink preparation process followed the same methodology outlined in Chapter 2, which involved the incorporation of glass microballoons into the epoxy resin system, followed by thorough mixing, degassing, and rheological optimization to ensure suitable printability for the Direct Ink Writing (DIW) process.

The 3D printing of the hexagonal honeycomb specimens was conducted using the same DIW setup and printing conditions described in Chapter 2. This included the use of a pneumatic-driven extrusion system, a nozzle diameter of 0.41 mm, a constant printing speed of 10 mm/min, and a layer height of 0.41 mm. The print parameters were selected to maintain consistency with previous tensile and compressive specimen fabrication to enable meaningful performance comparisons.

Three-dimensional models of the hexagonal honeycomb structures were designed using SOLIDWORKS. The honeycomb geometry was designed with a 30% infill density and consisted of a repeating hexagonal cell pattern optimized for lightweight structural applications. The corresponding STL files were exported and processed using open-source slicing software, including Slic3r and Repetier-Host, to generate the initial G-code for printing.

The generated G-code was subsequently customized to optimize the continuity of the print path and minimize non-printing movements within and between layers. Specific attention was given to tailoring the multi-stroke print-path strategy to reduce start-stop extrusion inconsistencies and enhance the overall structural integrity of the printed honeycomb cores. Figure 25 illustrates the 3D printing process and highlights the multi-stroke path strategies implemented for the hexagonal honeycomb design.

4.2.1 3D Printing Process

Figure 25 illustrates the print path strategy developed for the 3D printed hexagonal honeycomb structures fabricated using the optimized iM30K_2 iM16K_2 hybrid ink formulation. The figure provides a detailed representation of the toolpath generated for the DIW process, highlighting the specific regions of print movement and non-print movement within each layer of the honeycomb core.

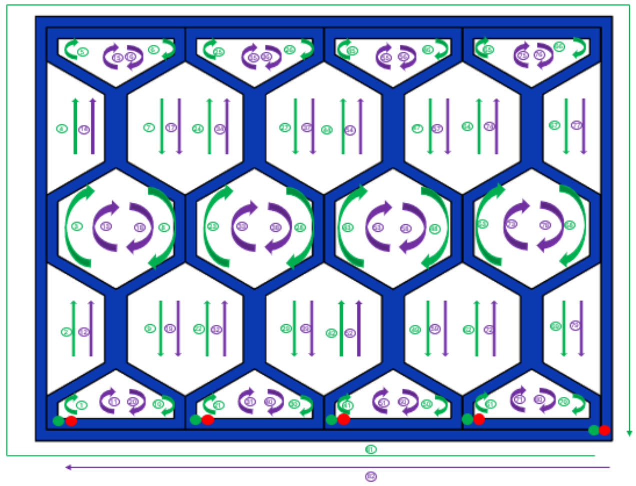

Figure 25:Print path for the 3D printed hexagonal honeycomb

In this figure, the green lines represent the print path, which corresponds to the continuous extrusion of material during printing. The print path was designed to follow a multi-stroke strategy that minimized start-stop extrusion events and optimized the continuity of the printed walls. This approach is critical in maintaining structural integrity and reducing the formation of defects, such as gaps or discontinuities, especially in complex geometries like honeycomb structures [29, 30].

The purple lines in Figure 25 represent the non-print path, indicating the travel movements of the print head where no material is deposited. Careful customization of the generated G-code was performed to minimize these non-printing movements within and between layers, reducing the potential for material stringing, nozzle drips, and other print artifacts that can compromise the mechanical performance of the final structure.

The print path strategy was designed such that the external boundary walls of the honeycomb were printed first to define the overall shape of the part. Subsequently, the inner hexagonal walls were printed using a combination of linear and circular toolpaths to efficiently fill the interior regions while maintaining geometric accuracy. The multi-stroke approach used for the infill regions allowed for better control of extrusion pressure, reduced nozzle retraction events, and improved filament overlap at junction points.

4.2.2 Compression Testing of Hexagonal Honeycomb

Compression testing was conducted to evaluate the in-plane compressive properties of the 3D printed hexagonal honeycomb structures fabricated using the optimized iM30K_2 iM16K_2 hybrid ink formulation. All compression tests were performed using an Instron universal testing system equipped with a 5 kN load cell, ensuring accurate force measurements while preventing overloading of the printed specimens. A constant crosshead displacement rate of 1 mm/min was applied throughout the testing procedure, following the same test conditions used for the previous compressive characterization of bulk samples discussed in Chapter 3.

Compression testing was carried out in both the X and Y in-plane directions to evaluate the anisotropic behavior of the printed honeycomb cores. The X-direction corresponds to loading parallel to the horizontal cell walls, while the Y-direction corresponds to loading parallel to the vertical cell walls. Figure 26 shows representative images of the honeycomb specimens positioned within the compression platens of the Instron machine prior to testing. Figure 26 shows a specimen oriented for Y-direction (a) and X-direction compression.

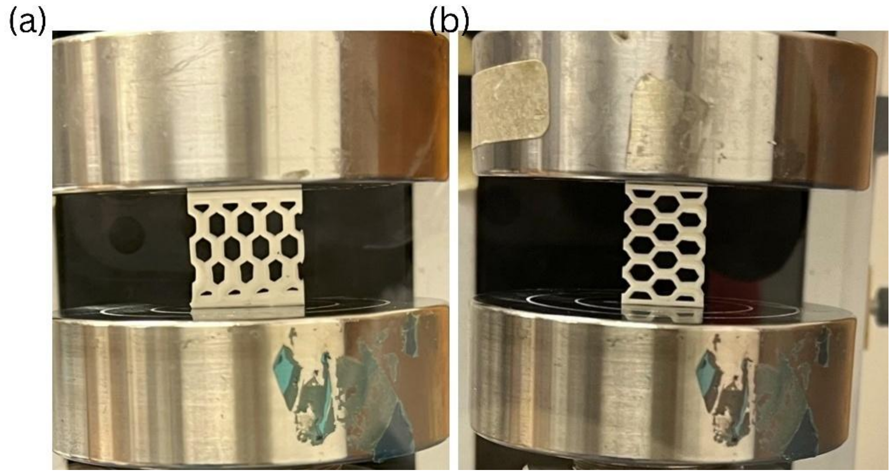

Figure 26: Experimental Set-Up for testing hexagonal honeycomb core

4.3 In-Plane Compressive Properties of Hexagonal Honeycomb Core

The primary compressive properties evaluated from the stress-strain response included peak specific compressive strength, specific compressive modulus. These properties provide critical insight into the load-bearing performance and energy dissipation behavior of the printed honeycomb structures. Testing in both directions was essential to assess the potential anisotropy introduced by the honeycomb geometry and print path strategy, and to validate the performance of the iM30K_2 iM16K_2 hybrid ink in complex structural applications.

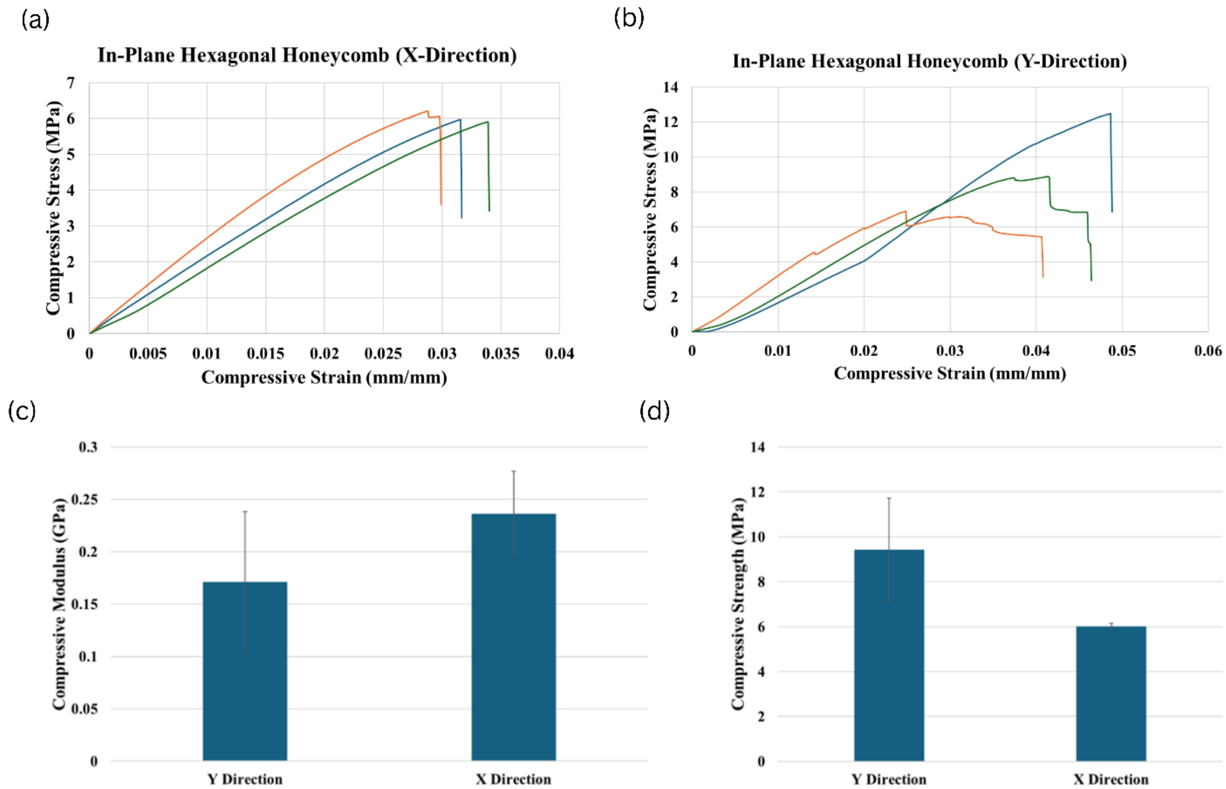

Figure 27: Compressive stress versus strain response of the 3D printed hexagonal honeycomb core structures in both X and Y in-plane directions

The compressive stress versus strain response of the 3D printed hexagonal honeycomb core structures in both the X and Y in-plane directions is shown in Figures 27 (a) and (b). The compressive modulus results, shown in Figure 27 (c), indicated that the X-direction specimens exhibited a slightly higher average modulus of 0.236 GPa compared to 0.171 GPa for the Y-direction specimens. The difference in stiffness between directions was relatively small, suggesting that the honeycomb geometry and multi-stroke print strategy provided good structural uniformity and minimized directional dependence in stiffness.

In contrast, the peak compressive strength results, shown in Figure 27 (d), demonstrated that the Y-direction specimens outperformed the X-direction specimens, with an average peak strength of

9.423 MPa compared to 6.020 MPa in the X-direction. This behavior is expected for hexagonal honeycomb structures, as the Y-direction corresponds to loading along the vertically aligned cell walls, which provide a more direct and continuous load path for compressive loading. These vertically aligned walls enhance load-bearing capacity, delay the onset of local buckling, and enable higher peak compressive strength. In contrast, the X-direction corresponds to loading across the inclined cell walls, which results in a more deformation-dominated response. In this orientation, load transfer is less direct, and the inclined walls are more susceptible to early buckling or folding, leading to lower peak strength. Additionally, the Y-direction loading benefits from increased filament-to-filament contact points aligned with the loading axis, further contributing to its superior load-bearing performance.

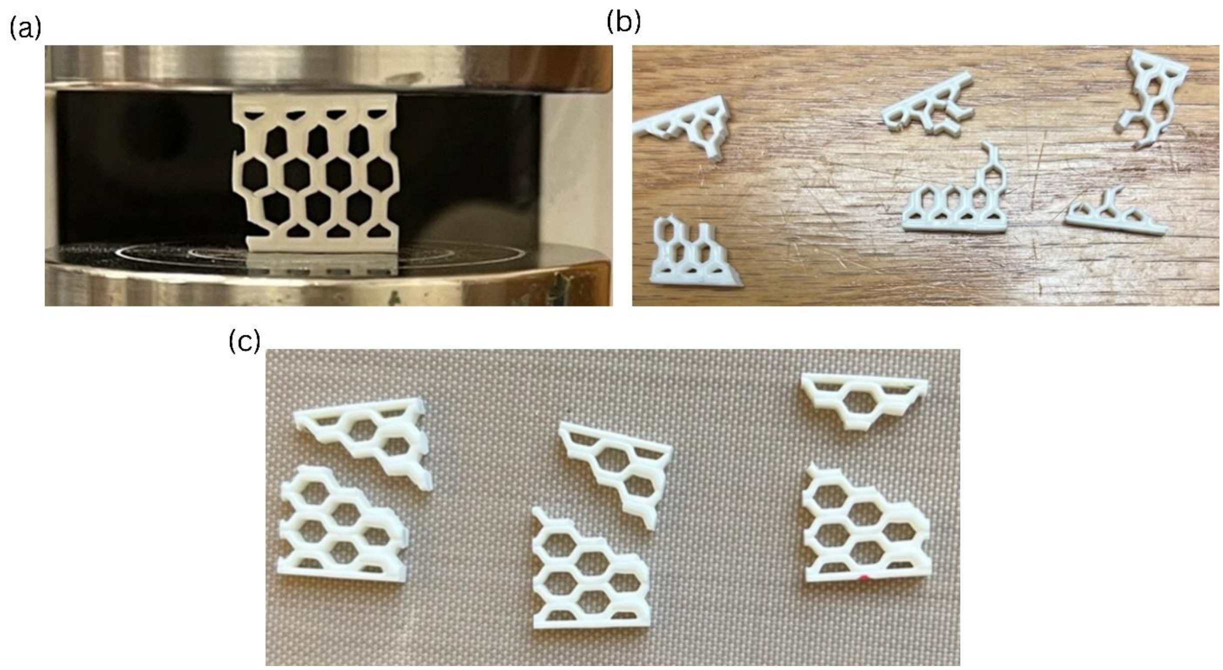

Figure 28: Fractured Specimen for (a)-(b) Y-direction, (b) X-direction tested specimen

Figure 28 illustrates the compressive testing and post-failure states of 3D printed honeycomb structures under in-plane loading. Figure 28 (a) shows the specimen loaded in the Y-direction, where progressive failure initiated in the bottom-left corner, indicating localized buckling and gradual collapse of cell walls as the load increased. This behavior suggests enhanced energy dissipation through controlled deformation, rather than abrupt fracture. Figure 28 (b) displays the final failed Y-direction specimen, with fragments showing asymmetric damage and partial crushing, consistent with a progressive failure mode that unfolded across multiple cells.

In contrast, X-direction loading resulted in a more brittle failure mode, characterized by a consistently inclined failure pattern, as shown in Figure 28 (c). The sharp and uniform angle of fracture across specimens indicates a shearing-dominated collapse with minimal plastic deformation. This brittle behavior implies limited energy absorption, with the load-bearing capacity rapidly compromised after initial failure. Collectively, these observations highlight the anisotropic mechanical response of the printed honeycomb architecture, with Y-direction compression offering greater structural resilience through staged collapse, and X-direction compression leading to sudden, catastrophic failure.

In terms of specific properties, the specific strength of the Y-direction specimens was calculated as 0.0232 MPa/(kg/m^3), outperforming the X-direction value of 0.0130 MPa/(kg/m^3). This further highlights the advantage of loading parallel to the vertically aligned cell walls in the honeycomb geometry. However, the specific modulus values were slightly higher in the X-direction at 0.00051 GPa/(kg/m^3) compared to 0.00042 GPa/(kg/m^3) for the Y-direction. This trend aligns with the observed modulus results and reflects the structural efficiency of the honeycomb design, where the X-direction walls provide slightly higher stiffness but lower ultimate strength.

Overall, these results demonstrate that the iM30K_2 iM16K_2 hybrid ink honeycomb structures exhibited excellent in-plane compressive performance, with the Y-direction providing superior load-bearing capacity due to the alignment of the cell walls with the loading direction, while maintaining comparable stiffness and deformation characteristics in both directions. These findings validate the suitability of the developed hybrid ink for use in lightweight, energy-absorbing structural core applications.

4.4 Chapter Conclusion

This chapter presented the fabrication, testing, and mechanical characterization of 3D printed hexagonal honeycomb core structures using the optimized hybrid epoxy syntactic foam ink formulation (iM30K_2 iM16K_2). The objective was to evaluate the in-plane compressive performance of the printed honeycomb structures and validate the suitability of the developed material for lightweight structural applications.

The honeycomb structures were successfully designed in SOLIDWORKS and fabricated using the Direct Ink Writing (DIW) process under the same printing conditions and methodologies outlined in previous chapters. Customized multi-stroke print path strategies were implemented to minimize non-printing movements and enhance print continuity and structural integrity.

Compression testing was conducted in both the X and Y in-plane directions to assess the potential anisotropy in mechanical behavior due to honeycomb geometry. The compressive stress-strain response of the printed honeycomb structures exhibited predominantly brittle behavior, with failure occurring shortly after the initial linear elastic region. Unlike traditional polymeric foams or metallic honeycombs, no distinct plateau region associated with progressive cell wall buckling was observed. Instead, once the elastic limit was reached, rapid failure occurred, characterized by fracture of the printed walls and collapse of the cellular structure.

Despite the brittle failure behavior, meaningful differences were observed between the X and Y loading directions. The X-direction exhibited a slightly higher compressive modulus of 0.236 GPa compared to 0.171 GPa for the Y-direction, indicating comparable stiffness across both directions. However, the Y-direction demonstrated a higher peak compressive strength of 9.423 MPa relative to 6.020 MPa for the X-direction. This difference is attributed to the honeycomb geometry, where the Y-direction loading engages the inclined cell walls, allowing for higher load redistribution before catastrophic failure.

Specific property evaluation further emphasized the lightweight efficiency of the printed honeycomb cores. The specific strength was higher in the Y-direction (0.0232 MPa/(kg/m^3)) compared to the X-direction (0.0130 MPa/(kg/m^3)), consistent with its higher load-bearing capacity. In contrast, the specific modulus was slightly higher in the X-direction (0.00052 GPa/(kg/m^3)) compared to the Y-direction (0.00041 GPa/(kg/m^3)), aligning with the observed stiffness trends.

Overall, the results demonstrated that the iM30K_2 iM16K_2 hybrid ink, combined with a controlled DIW printing process and optimized honeycomb geometry, produced lightweight structures with a balanced trade-off between stiffness, strength, and weight savings. The brittle failure mode observed highlights the inherent limitations of epoxy-based syntactic foam structures in energy-absorbing applications but confirms their suitability for lightweight load-bearing core structures where stiffness and strength are prioritized.

The findings of this chapter validate the effectiveness of the developed material system and printing strategies, providing a foundation for future work aimed at improving toughness, optimizing cellular designs, or incorporating energy-absorbing mechanisms into 3D printed syntactic foam structures.

Chapter 5: Conclusion and Future Work

This thesis focused on the development, characterization, and mechanical evaluation of 3D printed epoxy syntactic foams using Direct Ink Writing (DIW) technology for lightweight structural applications. Three distinct epoxy syntactic foam inks were formulated using EPON 815C epoxy resin combined with three different grades of hollow glass microballoons (GMBs): S60, iM16K, and iM30K. The ink formulation strategy incorporated fumed silica and thixotropic additives to optimize rheological behavior for printability.

Rheological characterization confirmed that all inks exhibited desirable shear-thinning behavior, with viscosity decreasing significantly with increasing shear rate which is a critical requirement for DIW printing. Amplitude sweep tests further demonstrated that the iM16K ink exhibited the highest yield stress due to its highest volume fraction of microballoons, while S60 exhibited the lowest yield stress due to its larger particle size and lower volume fraction.

Mechanical characterization of both cast and 3D printed specimens was conducted to evaluate tensile and compressive properties. Cast specimens showed higher variability and evidence of defects such as voids due to the challenges of casting highly viscous, particle-filled systems. In contrast, 3D printed specimens exhibited more consistent mechanical performance, highlighting the advantage of DIW processing for these materials.

Tensile testing demonstrated the influence of print orientation on mechanical properties, with 0° printed dogbone specimens generally exhibiting the highest tensile modulus and strength due to filament alignment with the loading direction. However, in some cases, 90° printed specimens outperformed 0° specimens, likely due to reduced defects in cross-layer deposition.

Compressive testing of unidirectional and bidirectional printed cubes revealed the anisotropic behavior of the syntactic foam structures. Loading in the direction parallel to the print lines (X-direction) generally resulted in higher stiffness, while the Y-direction often exhibited higher peak stress due to better stress distribution across inclined walls.

Hybrid inks were formulated by combining iM16K and iM30K microballoons in varying ratios (3:1, 2:2, 1:3). The hybrid ink with a 2:2 ratio (iM30K_2 iM16K_2) demonstrated the most balanced mechanical performance, achieving the highest specific strength and specific modulus values, as well as superior crashworthiness parameters including energy absorption (EA), specific energy absorption (SEA), mean crushing force (MCF), and peak crushing force (PCF).

Finally, a hexagonal honeycomb structure was designed and printed using the optimal hybrid ink (iM30K_2 iM16K_2). In-plane compression testing revealed direction-dependent behavior, with the Y-direction outperforming the X-direction in peak compressive strength due to loading along vertically aligned cell walls. These findings validated the material formulation and DIW printing strategy developed in this work for lightweight structural core applications.

While this study established a robust framework for developing and characterizing 3D printed epoxy syntactic foams, several avenues for future work are recommended:

1. Toughening Strategies

Although the developed inks exhibited high strength and stiffness, the failure behavior remained predominantly brittle. Future work could explore the incorporation of toughening agents such as rubber particles, thermoplastic additives, or nanoparticles to improve fracture toughness and energy absorption capacity.

2. Multi-Scale Reinforcement

Integrating multi-scale reinforcements, such as carbon nanotubes (CNTs) or graphene, alongside glass microballoons may offer synergistic improvements in mechanical performance while retaining lightweight properties.

3. Out-of-Plane Compression Testing

This study primarily focused on in-plane compressive behavior of printed honeycomb structures. Future work should investigate out-of-plane compression performance to further evaluate the structural efficiency of the syntactic foam cores under multi-directional loading.

4. Optimization of Print Path Strategies

Further exploration of G-code optimization techniques, including variable filament width, alternate raster patterns, or gradient printing of microballoon concentrations, could lead to improved mechanical anisotropy control and structural integrity.

5. Functionalization or Surface Treatment of Microballoons

Surface treatment or functionalization of glass microballoons (e.g., silane coupling agents or POSS coatings) could improve the interfacial bonding between the epoxy matrix and microballoons, potentially enhancing mechanical properties and reducing premature failure.

6. Long-Term Durability Studies

Future research should explore the long-term durability of printed syntactic foams, including environmental aging, thermal cycling, and moisture absorption studies, to assess their suitability for real-world structural applications.

References

[1] J. Ding et al., "Imperfection-enabled strengthening of ultra-lightweight lattice materials," *Adv. Sci.*, vol. 11, no. 41, 2024. doi: 10.1002/advs.202402727.

[2] W. Zhao, Y. Li, Q. Li, Y. Wang, and G. Wang, "Investigation of the structure-property effect of phosphorus-containing polysulfone on decomposition and flame retardant epoxy resin composites," *Polymers*, vol. 11, no. 2, p. 380, 2019. doi: 10.3390/polym11020380.

[3] L. O. Afolabi, Z. M. Ariff, S. F. S. Hashim, T. Alomayri, S. Mahzan, K.-A. Kamarudin, and I. D. Muhammad, "Syntactic foams formulations, production techniques, and industry applications: a review," *J. Mater. Res. Technol.*, vol. 9, no. 5, pp. 10698–10718, 2020. doi: 10.1016/j.jmrt.2020.07.057.

[4] N. Gupta and R. Nagorny, "Tensile properties of glass microballoon-epoxy resin syntactic foams," *J. Appl. Polym. Sci.*, vol. 102, no. 2, pp. 1254–1261, 2006. doi: 10.1002/app.23548.

[5] K. Dando, W. Cross, M. Robinson, and D. Salem, "Production and characterization of epoxy syntactic foams highly loaded with thermoplastic microballoons," *J. Cell. Plast.*, vol. 54, no. 3, pp. 499–514, 2017. doi: 10.1177/0021955x17700093.

[6] J. Restrepo and H. Colorado, "Additive manufacturing of composites made of epoxy resin with magnetite particles fabricated with the direct ink writing technique," *J. Compos. Mater.*, vol. 54, no. 5, pp. 647–657, 2019. doi: 10.1177/0021998319865019.

[7] A. Mondal, M. C. Saha, Y. Jiang, D. Rhule, and J. E. C. Sabisch, "Direct ink writing of hexagonal honeycomb carbon fiber-reinforced epoxy composites with varying cell geometric

parameters and tailored in-plane compressive properties," *Polym. Compos.*, pp. 1–18, 2025. doi: 10.1002/pc.29767.

[8] R. Chitrakar, M. Hossain, and S. Nilufar, "The effect of microballoon volume fraction on the elastic and viscoelastic properties of hollow microballoon-filled epoxy composites," *Materials*, vol. 16, no. 24, p. 7554, 2023. doi: 10.3390/ma16247554.

[9] J. Uranga, T. Carranza, M. Peñalba, K. Caba, and P. Guerrero, "Valorization of agar production residue as a filler in soy protein hydrogels for 3d printing," *Int. J. Bioprint.*, vol. 9, no. 4, p. 731, 2024. doi: 10.18063/ijb.731.

[10] R. Lemus-Mondaca et al., "Printability and thermophysical properties of three-dimensional-printed food based on “cochayuyo” durvillaea antarctica seaweed flour," *Foods*, vol. 13, no. 12, p. 1825, 2024. doi: 10.3390/foods13121825.

[11] S. Ahmadzadeh, T. Clary, A. Rosales, and A. Ubeyitogullari, "Upcycling imperfect broccoli and carrots into healthy snacks using an innovative 3d food printing approach," *Food Sci. Nutr.*, vol. 12, no. 1, pp. 84–93, 2023. doi: 10.1002/fsn3.3820.

[12] R. Woo, G. Chen, J. Zhao, and J. Bae, "Structure–mechanical property relationships of 3d-printed porous polydimethylsiloxane," *ACS Appl. Polym. Mater.*, vol. 3, no. 7, pp. 3496–3503, 2021. doi: 10.1021/acsapm.1c00417.

[13] P. Wei et al., "Go with the flow: rheological requirements for direct ink write printability," *J. Appl. Phys.*, vol. 134, no. 10, 2023. doi: 10.1063/5.0155896.

[14] C. Cipriani, Y. Shu, E. Pentzer, and C. Benjamin, "Viscoelastic and thixotropic characterization of paraffin/photopolymer composites for extrusion-based printing," *Phys. Fluids*, vol. 34, no. 9, 2022. doi: 10.1063/5.0104157.

[15] H. Tewani, D. Bonthu, H. Bharath, M. Doddamani, and P. Prabhakar, "Dynamic impact resistance of composite sandwich panels with 3-d printed polymer syntactic foam cores," presented at ASC 36, 2021. doi: 10.12783/asc36/35799.

[16] J. Ding, Q. Liu, F. Ye, H. Zhang, Y. Gao, and B. Zhang, "Compressive properties of co-continuous hollow glass microsphere/epoxy resin syntactic foams prepared using resin transfer molding," *J. Reinf. Plast. Compos.*, vol. 39, no. 3-4, pp. 132–143, 2019. doi: 10.1177/0731684419877568.

[17] P. Anandakumar, K. Kanny, T. Mohan, and V. Ramachandran, "Mechanical behavior of glass fiber-reinforced hollow glass particles filled epoxy composites under thermal loading," *J. Compos. Mater.*, vol. 58, no. 18, pp. 2027–2044, 2024. doi: 10.1177/00219983241259113.

[18] M. Attia, M. El-baky, M. Hassan, T. Sebaey, and E. Mahdi, "Crashworthiness characteristics of carbon–jute–glass reinforced epoxy composite circular tubes," *Polym. Compos.*, vol. 39, no. S4, 2017. doi: 10.1002/pc.24597.

[19] Q. Ding, X. Li, D. Zhang, G. Zhao, and Z. Sun, "Anisotropy of poly(lactic acid)/carbon fiber composites prepared by fused deposition modeling," *J. Appl. Polym. Sci.*, vol. 137, no. 23, 2019. doi: 10.1002/app.48786.

[20] Y. Chen et al., "Effect of printing parameters on interlayer bond strength of 3d printed limestone-calcined clay-based cementitious materials: an experimental and numerical study," *Constr. Build. Mater.*, vol. 262, p. 120094, 2020. doi: 10.1016/j.conbuildmat.2020.120094.

[21] A. Zandiatashbar et al., "Effect of defects on the intrinsic strength and stiffness of graphene," *Nat. Commun.*, vol. 5, no. 1, 2014. doi: 10.1038/ncomms4186.

[22] K. Gossaye et al., "Compressive behavior of habesha eggshell particulate reinforced epoxy composites," *Polym. Compos.*, vol. 44, no. 1, pp. 562–573, 2022. doi: 10.1002/pc.27119.

[23] A. Baroutaji, M. Sajjia, and A. Olabi, "On the crashworthiness performance of thin-walled energy absorbers: recent advances and future developments," *Thin-Walled Struct.*, vol. 118, pp. 137–163, 2017. doi: 10.1016/j.tws.2017.05.018.

[24] Y. Li et al., "Energy absorption characteristics and parameter optimization of anti-climb energy-absorbing devices for subway vehicles under impact loads," *Appl. Sci.*, vol. 14, no. 12, p. 5203, 2024. doi: 10.3390/app14125203.

[25] D. Mu, X. Hu, H. Yu, and B. Yu, "Investigation of ultrasonic-assisted cnc cutting of honeycomb cores," *Int. J. Adv. Manuf. Technol.*, vol. 117, no. 3-4, pp. 1275–1286, 2021. doi: 10.1007/s00170-021-07820-x.

[26] Y. Lin et al., "Cushioning and energy absorbing property of combined aluminum honeycomb," *Adv. Eng. Mater.*, vol. 17, no. 10, pp. 1434–1441, 2015. doi: 10.1002/adem.201400574.

[27] Y. Chen, R. Das, and M. Battley, "Experimental study on in-plane compressive response of irregular honeycombs," *J. Compos. Mater.*, vol. 52, no. 8, pp. 1121–1135, 2017. doi: 10.1177/0021998317749964.

[28] L. Tripathi and B. Behera, "Flatwise compression behavior of 3d woven honeycomb composites," *J. Ind. Text.*, vol. 52, 2022. doi: 10.1177/15280837221125483.

[29] S. Jain et al., "Engineering 3d degradable, pliable scaffolds toward adipose tissue regeneration; optimized printability, simulations and surface modification," *J. Tissue Eng.*, vol. 11, 2020. doi: 10.1177/2041731420954316.

[30] F. Yang, M. Zhang, B. Bhandari, and Y. Liu, "Investigation on lemon juice gel as food material for 3d printing and optimization of printing parameters," *LWT*, vol. 87, pp. 67–76, 2018. doi: 10.1016/j.lwt.2017.08.054.